

---

## Observed and projected Sea Surface Temperature seasonal changes in the Western English Channel from satellite data and CMIP5 multi-model ensemble.

L'Hévéder Blandine <sup>1,\*</sup>, Speich Sabrina <sup>2</sup>, Ragueneau Olivier <sup>1</sup>, Gohin Francis <sup>3</sup>, Bryère Philippe <sup>4</sup>

<sup>1</sup> LEMAR, IUEM Technopôle Brest-Iroise, rue Dumont d'Urville, 29280 Plouzané, FRANCE

<sup>2</sup> LMD, ENS, 24 rue Lhomond, 75231 Paris cedex 05, FRANCE

<sup>3</sup> IFREMER/DYNECO/PELAGOS, Centre Ifremer de Brest, 29280 Plouzané, FRANCE

<sup>4</sup> ACRI-HE, 40 Quai de la douane, 29200 Brest, France

\* Corresponding author : Blandine L'Hévéder, email address : [blandine.lheveder@lmd.jussieu.fr](mailto:blandine.lheveder@lmd.jussieu.fr)

---

### Abstract :

Seasonal Sea Surface Temperature (SST) changes in the Western English Channel have been estimated for the previous decades from high-resolution satellite data. Coastal seas, well separated from offshore waters by intense frontal structures, show colder SST by 1 to 2°C in summer. A significant warming trend is observed in the autumn season. This positive trend is stronger offshore, with an annual mean SST increase of 0.32°C/decade, but weaker in coastal waters (0.23°C/decade), where strong vertical mixing induced by tides and winds acts to reduce surface warming. The performance of an ensemble of CMIP5 climate model in simulating recent seasonal changes of SST in the region is estimated. The median of CMIP5 models reproduces very well the observed SST mean seasonal cycle in offshore waters but is less proficient in the coastal sector due to the coarse resolution of the models and the absence of tidal forcing and related processes. In the Iroise Sea, a region of intense biological activity located off the western tip of Brittany, the trend of the annual mean SST is relatively well simulated, albeit somewhat underestimated (0.20°/decade) and evenly distributed throughout the year. Here, the increase in annual mean SST in CMIP5 future scenarios simulations ranges from 0.5°C (RCP2.6) to 2.5°C (RCP8.5) by year 2100, with a seasonal modulation leading to a more intense warming in summer than in winter. This increase in SST may strongly affect marine biology, particularly phytoplankton phenology, macro-algae biomass and benthic fauna, including exploited shellfish, in the Western English Channel.

**Keywords :** SST, Climate change, Western English Channel, CMIP5, regional study

## 40           **1. Introduction**

41           Climate change will affect marine ecosystems in many different ways, through the alteration of the  
42           physical environment, biogeochemical cycles, biodiversity, and hence ecosystem structure and  
43           functioning (IPCC, 2014). The impact of climate change on biodiversity includes profound changes in  
44           species distribution and abundance, leading to global extinction and alteration of ecosystem services  
45           (Bellard et al., 2012). As a result of that, society, and in particular coastal communities, have to adapt  
46           to these changes (Millennium Ecosystem Assessment, 2005). In order to move towards adaptation and  
47           mitigation, there is a crucial need to improve the predictive capacity of models to depict future  
48           changes in the physical environment, especially at local or regional scale. Among the most crucial  
49           parameters to be studied, is sea surface temperature (SST). Temperature plays a fundamental role in  
50           ocean processes (circulation, stratification), in controlling the thermodynamic and kinetic  
51           characteristics of chemical and biogeochemical processes (degradation, dissolution, precipitation), in  
52           controlling the spatial distribution, the metabolic rates and the life cycle of marine flora (Bissinger et  
53           al., 2008; Chen, 2015) and fauna (Southward et al., 1995; Helmuth et al., 2006; Philippart et al, 2011;  
54           Thomas et al., 2016). The region of interest for this study is the Western English Channel, an oceanic  
55           region located off the western coasts of France, including the English Channel to the north, the Iroise  
56           Sea in the central-west portion and the Bay of Biscay at the southern end (Figure 1). Inside, two  
57           oceanic areas can be identified with different sea temperature sensitivities to global change. The first  
58           one, composed of the southern Brittany and the offshore waters of the Western English Channel,  
59           shows a seasonal stratification with frequent occurrences of a strong summer bloom of the harmful  
60           dinoflagellate *Karenia mikimotoi* on the warm side of the seasonal front of SST (Vanhoutte-Brunier et  
61           al., 2008, Hartmann et al., 2014). The second part of the region, essentially coastal but including also  
62           the central English Channel, is vertically well-mixed by tides (Gohin et al., 2015). In this area, a small  
63           increase in the water temperature could have a dramatic effect on the kelp *Laminaria digitata*, which is  
64           on the verge of local extinction due to the increase in sea temperature (Méléder et al., 2010, Raybaud  
65           et al., 2013). This is also a biogeographic boundary zone and, in recent years, warm water species

66 have become much more common (Southward, 1980 ; Southward et al., 1995 ; Hawkins et al., 2003 ;  
67 Southward et al., 2005 ; Hawkins et al., 2008 ; Smale et al., 2013). Ecological problems related to SST  
68 change in the Western English Channel also include the alteration of nutrient delivery from land to  
69 sea, development of invasive species such as *Crepidula fornicata*, *Spartina sp.*, *Crassostrea giga*,  
70 alteration of host–pathogen relationships and biological interactions (Poloczanska et al., 2008).  
71 Biologists try to better understand the response of these populations to increasing SST (Altizer et al.,  
72 2013).

73 There is a long history of research on the impacts of SST fluctuations on marine flora and fauna in  
74 the Western English Channel (Southward et al., 2005). The studies have shown both warm (1880–  
75 1890s, 1930–1950s) and cold periods (1960s to mid 1980s) before the recent period of rapid warming  
76 driven by anthropogenic climate change. The time window studied here is the one of recent warming.  
77 Over the last 30 years, the average surface temperature of the North Atlantic has risen (Rhein et al.,  
78 2013). This trend is not uniform because of regional variability, and not all areas of the Northeast  
79 Atlantic show the same long–term trends. However, the warming tendency of surface waters off the  
80 coasts of Brittany is similar to the North Atlantic average temperature trend (Dye et al., 2013). In the  
81 shallow seas of the Western English Channel, there is also substantial evidence of a warming over the  
82 past decades inferred from satellite observations (Cannaby and Hüsrevoglu, 2009, Saulquin and Gohin,  
83 2010, Dye et al., 2013) and from regional modelling studies (Michel et al., 2009, Holt et al., 2012). On  
84 the wide northwest European continental shelf, global warming is modulated by mesoscale oceanic  
85 processes, resulting in spatial patterns of SST that differ by their seasonal cycle, variability and trend.

86 To predict future climate change impacts on coastal ecosystems over the 21st century, an  
87 assessment of the sea temperature evolution is necessary. In the framework of the IPCC's 5th report,  
88 projections of future climate change have been made for several socio–economical scenarios with an  
89 ensemble of Earth System Models (ESM). Nevertheless, ESMs invariably give a very poor  
90 representation of the land–ocean interface and of the shelf seas. The reasons for this are twofold: first,  
91 the resolution and, second, the representation of physical processes including the shelf sea barotropic

92 processes or the long gravity waves associated with tides and wind-generated coastally trapped waves  
93 (Holt et al., 2009). Besides, there are few published regional model simulations with sufficient  
94 resolution to include shelf sea processes (e.g. tidal mixing fronts and coastal currents) and of sufficient  
95 duration to investigate how atmospheric and/or oceanic fluxes drive the interannual to decadal  
96 variability. Focusing on regional models including our study region --that is the French Atlantic  
97 shoreline and the English Channel-- only two simulations cover the recent past. Holt et al. (2012)  
98 have modelled the temperature over the European continental shelf with the Atlantic Margin  
99 configuration of POLCOMS at 12 km resolution over the period 1960–2002. Michel et al. (2009) have  
100 analyzed the temperature variability in the Bay of Biscay through a simulation performed with a global  
101 configuration of NEMO (resolution of  $\sim 20$  km, but tides not simulated) for the period 1958–2004.  
102 Besides that, a higher number of modelling studies have been undertaken to model the changes in  
103 ocean properties in the North Sea (Schrum, 2001, Meyer et al., 2011, Hjøllø et al., 2009 ) and in the  
104 Irish Sea (Young and Holt, 2007) over the previous decades.

105           Downscaling of climate change scenarios have also been performed over the European  
106 continental shelf. Adlandsvik (2008) has compared a global climate simulation implemented with the  
107 BCM model under the SRES–A1B scenario (IPCC, 2007) with the associated downscaled simulation  
108 with ROMS over the North Sea at 8 km resolution. Later on, Friocourt et al. (2012) have used two  
109 hydrographic models for the downscaling of the same scenario over the North Sea, but only for a 20–  
110 year period in the near future (2040s). Their study covers also the impacts on the phytoplankton  
111 blooms using an ecological model. In the Irish Sea, Olbert et al. (2012) have downscaled the SRES–  
112 A1B scenario using ECOMSED model at 2km resolution. Finally, regarding our region of interest, an  
113 ocean simulation of the European continental shelf has been performed with the regional ocean model  
114 POLCOMS (at 12 km resolution) nested in the ESM HadCM3 under the SRES–A1B scenario (Holt et  
115 al., 2010). Only the latter study covers the French Atlantic shoreline and the English Channel. It is  
116 therefore necessary to go further and to investigate the variety of climate models responses to future  
117 climate change in this region. Following Hawkins and Sutton (2009), the dominant sources of

118 uncertainty for surface temperature prediction at regional scale are model and scenario uncertainties,  
119 for time horizons of many decades or longer. To reduce model uncertainty, Foley (2010) has  
120 demonstrated the efficiency of multi-model ensemble analysis.

121 The aim of this work is to evaluate the seasonal changes for SST in the Western English  
122 Channel in the previous decades (1980–now) and up to the end of the 21st century. To take into  
123 account the issues of uncertainty, we choose to analyze a multi-model ensemble of global climate  
124 models from the Coupled Model Intercomparison Project Phase 5 (CMIP5; Taylor et al., 2012), for  
125 three Representative Concentration Pathway (RCP) scenarios (IPCC, 2014). For the previous decades,  
126 the warming trend detected in CMIP5 models is validated by that estimated from satellite data, in the  
127 three seas around Brittany at the grid scale of the models (~100 km). Then, changes in the SST  
128 seasonal cycle are assessed from the projections of CMIP5 models for future climate. The paper is  
129 organized as follows. In Section 2, the data sets and methodology are described. In Section 3, an  
130 overview of the changes in the SST seasonal cycle around Brittany over the last decades is presented.  
131 Then, future changes are estimated for the Iroise Sea, region of special interest for its intense  
132 biological activity. Section 4 addresses the expected impacts of the SST changes on the marine  
133 ecosystems and concludes.

## 134 2. Data Sets and methodology

### 135 2.1 CMIP5 climate models

136 Daily SST fields have been retrieved from the Earth System Grid (ESG) data portal  
137 (<http://pcmdi9.llnl.gov/esgf-web-fe/>) for 13 CMIP5 models (cf. Table 1). Most of them are European  
138 models, in which the northern mid-latitude climate is likely to have been further validated. Only one  
139 (typically the first) ensemble member of each model is used. The past analysis is based on the  
140 historical simulation of the CMIP5 models for the period 1980–2005, and the future change on the  
141 projections for three RCP scenarios (RCP2.6, 4.5 and 8.5; Moss et al., 2010) over the period 2006–  
142 2100. The historical simulations employ historical changes in the atmospheric composition reflecting  
143 both anthropogenic and natural sources, and include time-evolving land cover information (Taylor et

144 al., 2012). Then, the peak-and-decline RCP2.6 scenario is designed to meet the 2° C global average  
145 warming target compared to pre-industrial conditions by 2100 (van Vuuren et al., 2011a). Radiative  
146 forcing in RCP4.5 peaks at about 4.5 W/m<sup>2</sup> in year 2100 (Thomson et al., 2011). RCP8.5 assumes a  
147 high rate of radiative forcing increase, peaking at 8.5 W/m<sup>2</sup> in year 2100 (Riahi et al., 2011).

148 Figure 1 pictures the regional seas located off the coasts of French Brittany : the English  
149 Channel, the Iroise Sea and the Bay of Biscay. Each of these seas has specific characteristics, linked  
150 to local topography, continental geometry, hydrology, and will be analyzed separately. Most of CMIP5  
151 oceanic models have a typical low spatial resolution, of about 110 km x 110 km at 48° N (see a typical  
152 CMIP5 grid cell on Figure 1), so that the regional seas are modelled by only some grid cells and  
153 shallow bathymetry is not well represented. The English Channel is not depicted in some models, nor  
154 is it connected to the North Sea in others (see detailed characteristics of the different grid  
155 topographies and geometries in Tab. 1). Tides and sub-mesoscale processes are not simulated but the  
156 complete ocean-atmosphere system is modelled, including heat and energy exchanges between ocean  
157 and atmosphere, essential to predict climate change. For each of the 13 CMIP5 ocean models, the grid  
158 points localized in each of these seas are selected, and daily SST data are spatially averaged to  
159 produce time series representative of the SST evolution in each sea.

## 160 2.2 Satellite observations and characteristic surface waters in Brittany's sea

161 A set of satellite data was used to validate the model-simulated SST around Brittany: the Ifremer  
162 SST data derived from AVHRR/Pathfinder products interpolated by kriging (Saulquin and Gohin,  
163 2010); the OSTIA data provided by the Met Office using the Operational SST and Sea Ice Analysis  
164 (OSTIA) system described in Donlon et al. (2011); and the ODYSSEA data, also derived from multi-  
165 sensor data set incorporating microwave instruments, provided by MyOcean (Autret and Piollé, 2011).  
166 A daily time series for the period 1986–2013 of high-resolution SST satellite data was obtained by  
167 concatenating Ifremer AVHRR -derived SST data for 1986–2009, OSTIA data for 2010 and ODYSSEA  
168 data for 2011–2013. A comparison with an homogeneous time series covering the entire period,  
169 stemming from global low-resolution GHRSSST, showed that the inhomogeneity of the high-resolution

170 time series used here did not generate bias. The three sets of SST data were projected onto the same  
171 regular grid ---  $0.075^\circ$  in longitude and  $0.05^\circ$  in latitude --- allowing a high spatial resolution of  
172 about 5 km x 5 km.

173 Analyzing the Ifremer AVHRR-SST satellite data over 1986–2006, Saulquin and Gohin (2010)  
174 have shown that the mean annual warming of the SST was not spatially uniform in the English Channel,  
175 due to local physical and hydrodynamic oceanic processes. Indeed, fronts develop in summer and  
176 autumn, delimiting at the surface a warm area --at the north west of the Ushant front-- from a cold  
177 one, both differing also in their vertical structure. The area with a warm surface layer lies in thermally  
178 stratified open waters, while cold surface water lies in tidally mixed coastal waters. Figure 1 shows a  
179 snapshot of the SST on 18th June 2003, where sharp discontinuities in SST can be observed in the  
180 middle of the English Channel as well as in Iroise Sea (Iroise front) and off Ushant (Ushant front), with  
181 SST differences across the fronts of about  $2^\circ$  C. These fronts and their formation process have been  
182 long and extensively studied (Pingree and Griffiths, 1978 ; Simpson et al., 1978 ; Mariette and Le  
183 Cann, 1985 ; Le Boyer et al., 2009) and modelled (Muller et al., 2007 ; Cambon, 2008 ; Lazure et al.,  
184 2009).

185 To take into account the spatial inhomogeneity of the SST in the seas surrounding Brittany, areas  
186 with specific characteristics have been selected in each regional sea: « tidally mixed coastal waters »,  
187 hereafter denoted by TiMCW and « thermally stratified open waters », ThSOW. They are represented  
188 in Figure 1. In the Bay of Biscay, tides are weaker and mainly ThSOW are observed.

189  
190 Above all, a comparison of the satellite data spatially averaged to the same spatial scale as CMIP5  
191 models is essential, in order to smooth the sub-mesoscale variability present in the satellite data but  
192 not simulated in the models. For each of the three seas, a time series representing the large scale  
193 behaviour of the satellite SST has been computed as its average over ThSOW and TiMCW boxes.

194 2.3 Methodology

195           The end-to-end methodology applied to the Iroise Sea is the following. A set of indices is defined  
196 to characterize the SST seasonal cycle. They are computed from daily CMIP5 models data and high-  
197 resolution satellite data, spatially averaged to typical model grid scale. A « portrait diagram » of the  
198 different models performances to simulate the climatologic present-day observed SST seasonal cycle is  
199 shown, based on the indices. Over the last decades, trends in the indices are estimated in models and  
200 satellite data, to evaluate the past changes in the SST seasonal cycle and test their simulation in the  
201 models. Finally, future changes in the SST seasonal cycle are estimated from CMIP5 projections.

### 202           2.3.1 Indices for the SST seasonal cycle

203           In order to quantify the warming trend and the SST seasonal cycle change, indices are necessary.  
204 For the atmosphere, the Expert Team on Climate Change Detection and Indices (ETCCDI) has defined  
205 a set of climate indices that provide a comprehensive overview of temperature and precipitation  
206 statistics focusing particularly on extreme aspects (Karl and Easterling, 1999, Klein Tank et al., 2009).  
207 Multivariate Oceanic and Climatic Index (MOCI) have also been derived from a combination of global  
208 and regional climate indices to evaluate the impact of oceano-climatic changes on marine ecosystems  
209 in the Bay of Biscay (Hemery et al., 2008). So far, no set of indices has been developed for oceanic-  
210 only climatic characteristics.

211           We propose a set of 13 indices (defined in Table 2) to characterize the SST seasonal cycle. To  
212 compute these indices, daily data have been used to capture the most comprehensive signal. The  
213 time-averaged indices, I1 and I10 to I13, are directly computed from the daily time series. To estimate  
214 the indices I2 to I9, corresponding to the extremes (minimum, maximum) and time course (dates of  
215 minimum and maximum annual temperature, of spring and autumn onset) of the seasonal cycle,  
216 methodologies commonly applied to characterize the seasonal cycle of the temperature (Wyrтки, 1965,  
217 Eliseev and Mokhov, 2003, Saulquin and Gohin, 2010) have been used. Details on the computation are  
218 given in Table 2.

219

## 220 2.3.2 Trend estimate

221 To quantify the recent SST changes, linear trends in the SST monthly mean time series (Fig. 4)  
222 and in the indices time series (Figs. 5 to 7) were computed using a « Kendall's tau based slope  
223 estimator » developed by Wang and Swail (2001). This estimator is robust to the effect of outliers in  
224 the series and an iterative procedure prevents the Kendall test result from being affected by serial  
225 correlation of the series. This method has been widely used to compute trends in hydrometeorological  
226 series (e.g., Wang and Swail, 2001, Zhang et al., 2000) and taken up to estimate trends in climate  
227 extreme indices time series by Zhang et al. (2005). Throughout the paper, we only show trends  
228 considered as significant, taking a threshold level of 95%.

## 229 2.3.3 Model performance metrics

230 Given the large number of indices and models analyzed in this study, we have used a metric based  
231 approach to assess model performance, based on the estimation of « model relative error » of model  
232 climatologies (Gleckler et al., 2008) and adapted from Sillmann et al. (2013) application to climate  
233 extremes indices. This provides a synthetic overview of each model performance relative to the others  
234 for various indices characterizing the mean SST seasonal cycle under present-day climate.

235 The mean present-day SST seasonal cycle in CMIP5 models is assessed in the Iroise Sea, with  
236 respect to satellite observations over ThSOW and TiMCW (defined in Section 2.3.1). The indices are  
237 estimated at an annual frequency, as they characterize a feature of the annual cycle. For each index,  
238 we consider the climatology of its yearly time series over the common period between observations and  
239 models -- 1986-2004 --, at the model grid scale for models and averaged over ThSOW and TiMCW  
240 areas for satellite data. The climatologies are noted  $I_x$  for the model X and  $I_y$  for the satellite  
241 observations. The absolute value of the difference between models and observations climatologies is  
242 noted  $E_{xy} = |I_x - I_y|$ .

243 For each model X, the « model relative error »  $E'_{xy}$  is then derived from the collection of model-  
244 observation differences  $E_{xy}$  for all models as

$$E'_{xy} = \frac{E_{XY} - E_m}{E_m}$$

245

246

with  $E_m$  the median of the model–observation differences  $E_{xy}$  for all models.

247

248

$E'_{xy}$  provides an indication of the performance of the model X relative to the multi–model ensemble, with respect to satellite observations over an area in the Iroise sea. The median  $E_m$

249

represents typical model performance in the multi–model ensemble.  $E'_{xy}$  values for all models and all

250

indices obtained for both areas of the Iroise sea are summarized in a “portrait” diagram (Figure 3),

251

discussed in Section 3.1.2.

252

### 3. Results

253

#### 3.1 SST mean seasonal cycle in present–day climate

254

##### 3.1.1 SST mean seasonal cycle in satellite observations and CMIP5 multi–model ensemble

255

The SST mean seasonal cycle in satellite data and in CMIP5 historical simulations has been

256

evaluated for each of the three seas around Brittany (Figure 2). It is computed over the period 1980–

257

2005 for CMIP5 models and 1986–2013 for satellite data.

258

In the observations, as expected, the SST mean seasonal cycles in TiMCW and ThSOW differ in

259

summer and autumn. Due to the strong vertical mixing by tidal currents in coastal areas that prevents

260

the seasonal thermocline from establishing in summer (Pingree and Griffiths, 1978, Mariette and Le

261

Cann, 1985, Cambon, 2008), summer SSTs are colder in TiMCW than in ThSOW, with across front

262

differences of about 1° C in the English Channel to 2° C in the Iroise Sea. Surface ThSOW cool

263

earlier and faster in autumn, at the time when the seasonal thermocline disappears. In the TiMCW of

264

Iroise Sea and English Channel, the mean SST seasonal cycles of satellite data are in good agreement

265

with in situ–data from SOMLIT–Brest (at the outlet of the Bay of Brest) and SOMLIT–Astan (at the

266

outlet of the Bay of Morlay) (Tréguer et al., 2014).

267

In the three seas, the observed SST mean seasonal cycle in ThSOW is well simulated by the

268

median of CMIP5 models. Considering the low–resolution of climate models used here, it is important

269 to emphasize the absence of bias, distortion or shift in the median SST seasonal cycle of CMIP models,  
270 especially in the Iroise Sea. In summer, we notice a higher dispersion between model estimates, with an  
271 interquartile model spread ranging from 1.5° C in the Iroise Sea to 2° C in the English Channel. Each  
272 model taken individually presents a bias, but if we consider CMIP5 models simulations as an ensemble  
273 of climate simulations, the median of the ensemble represents well the observed SST mean seasonal  
274 cycle. However, a few differences to the observations can be noted. In the Bay of Biscay, summer SST  
275 are too warm by 1° C. In the English Channel, winter SST are too cold by 1° C. Finally, the  
276 characteristics of TiMCW --colder summer SST-- are not simulated in CMIP5 models. This is due to  
277 the absence of simulation of sub-mesoscale processes and tides in global models, dominant factors for  
278 the SST in TiMCW. In ThSOW, processes of air-sea interactions predomines for the SST estimate  
279 (Esnaola et al., 2012). The latter are relatively well simulated in CMIP5 ocean-atmosphere coupled  
280 models, even if air-sea processes associated with sub-mesoscale oceanic structures have been  
281 demonstrated to increase the heat and energy budget of the ocean surface waters (Hogg et al., 2009,  
282 Chelton and Xie, 2010).

### 283 3.1.2 Models performance inter-comparison for the Iroise Sea

284 An inter-comparison of the different CMIP5 models performance in the Iroise Sea, using the  
285 metrics described in Section 2.3.3, is shown on the portrait diagram (Figure 3). It represents the  
286 relative magnitude of the « model relative error » for each index (columns) and for each model (rows).  
287 The magnitudes of the « model relative errors » are colour-coded, with colder (resp. warmer) colors  
288 corresponding to  $E'_{xy} < 0$  (resp.  $E'_{xy} > 0$ ) for models getting a better (resp. poorer) performance than  
289 others on average. In the first two rows, the performance of the « mean » and « median » of the multi-  
290 model ensemble is also displayed.

291 In the portrait diagram, the mean and median of the CMIP5 multi-model ensemble get the better  
292 performance in representing the observed SST. This result is consistent with the conclusions of  
293 Gleckler et al. (2008), Sillmann et al. (2013) and other multi-model studies. Indeed, some of the  
294 systematic bias in each of the individual models are canceled out in the multi-model mean or median.

295 In ThSOW, the mean and median model index climatologies are really close to the observations, but  
296 less in TiMCW, thereby confirming the results and analysis of Section 3.1.1. Therefore, in the  
297 following, we focus on the evaluation of the models in ThSOW, more relevant. The models that  
298 better simulate the mean present-day SST seasonal cycle in the Iroise Sea are CNRM, ICHEC,  
299 HadCM3, MPI-MR and IPSL-MR. ICHEC, MPI-MR and CNRM have in common a higher ocean  
300 resolution and a more realistic topography and coastline geometry of the region of study than other  
301 models of the study; IPSL-MR, ICHEC and CNRM an higher atmospheric resolution. Regarding  
302 HadCM3, its good performance compared to HadGEM2-CC and HadGEM2-ES (the new generation of  
303 climate models of the MetOffice) is surprising also because the horizontal resolution has been refined  
304 in the recent ocean and atmosphere model versions. In the literature, Gordon et al. (2000) have  
305 demonstrated the very good skill of HadCM3 to simulate the SST with no flux adjustments, which was  
306 very novative at this time. By contrast, HadGEM2 (Collins et al., 2011) includes improvement  
307 designed to address specific systematic bias encountered in HadGEM1, namely Northern Hemisphere  
308 continental temperature biases, which may impact SST in the region of study. This result highlights the  
309 complexity of climate modelling in the fact that the realism of the simulations is not guaranteed to be  
310 improved by increasing the model resolution.

### 311 3.2 Change of SST seasonal cycle in the previous decades

#### 312 3.2.1 Overview of Western English Channel

313 The observed and modelled changes of the SST seasonal cycle in the last 30 years in the Western  
314 English Channel are illustrated in Figure 4. Time series for 1980–2013 of monthly mean SST in the  
315 satellite data (in ThSOW and in TiMCW) and in the CMIP5 models are produced for each of the seas  
316 located around Brittany. For each time series representing the evolution of the SST in a particular  
317 month, a monthly trend is shown if significant.

318 In the observations, a warming trend is visible in the last 30 years, concentrated during the  
319 autumn season. This autumn trend is present in both ThSOW and TiMCW. It is stronger in ThSOW,  
320 and reaches the maximum value of about  $0.6^{\circ}$  C/decade --- which gives a SST increase of  $1.8^{\circ}$  C in

321 30 years --- in the Iroise Sea and in the Bay of Biscay. In spring, in ThSOW, we note also a  
322 significant trend of about  $+0.3^{\circ}$  C/decade, this trend being more pronounced in the Iroise Sea. In  
323 TiMCW, the entire water column has to be warmed, which leads to a lower ocean surface warming. In  
324 summer, no significant trend can be detected, probably because of the higher interannual variability  
325 during that season.

326 In CMIP5 models historical simulations, the observed warming trend is simulated. However, in the  
327 Iroise Sea and in the English Channel, its seasonal distribution differs from the observed one. The  
328 warming trend is found all over the year, except during summer, with smaller values of about  
329  $0.25^{\circ}$  C/decade. In global models, the ocean surface warming trend seems more linearly linked to the  
330 greenhouse gases radiative forcing, because of the poor simulation of continental shelf processes. As  
331 pointed out by Holt et al. (2014) in their review paper, it is not just an issue of resolution: a suite of  
332 specific dynamic processes act in regional seas, which along with their particular geographic setting act  
333 to shape the climatic impacts and lead to responses that may be different from the wider global ocean.  
334 Indeed, Adlandsvik (2008), in a marine downscaling experiment of the SRES-A1B scenario over the  
335 North Sea, has demonstrated that downscaling strengthen the surface ocean warming. The regional  
336 model has a more realistic shelf sea stratification, and most of the warming can be trapped in the  
337 surface mixed layer during the summer season, resulting in a better seasonal distribution. In our study,  
338 we highlight the need to refine in the same way the spatial resolution and to model tides in the  
339 Western English Channel.

340 On the other end, the Bay of Biscay has smaller tides so that the oceanic characteristics are  
341 better simulated in climate models. Accordingly, the modelled warming trend seasonal distribution is  
342 closer to that of satellite observations, albeit half.

### 343 3.2.2 Trends of SST seasonal cycle indices in the Iroise Sea

344 To quantify changes in the SST seasonal cycle in the Iroise Sea in previous decades, the indices  
345 time series are shown in Figures 5 to 7, for the satellite observations averaged over the Iroise Sea,  
346 over the ThSOW and TiMCW areas, and for the median of the 13 CMIP5 simulations, with their

347 interquartile range. In the left column, the absolute values of the indices are presented. The SST gap  
348 between ThSOW and TiMCW in the Iroise Sea is highlighted, in particular in summer when the  
349 difference between the annual maxima reaches  $2.5^{\circ}$  C. Time series of ThSOW and TiMCW are highly  
350 correlated, pointing out the driving role of atmospheric surface forcing.

351 In the right column are shown the index anomalies relative to each index time-mean over 1986–  
352 2005, this being the common period between observations and models. For the multi-model ensemble,  
353 anomalies are first calculated separately for each model, by removing the index time-mean of the  
354 model simulation, and then the median of the models anomalies is computed. That way, the bias  
355 between the different data sets is eliminated and clearer trends emerge in the CMIP5 multi-model  
356 ensemble. For the models, we note that trends of index absolute values and anomalies differ often by  
357 15 to 30%. Trends of anomalies, not affected by the bias between the models and thus more  
358 representative of the variability, are discussed.

359 The annual mean of the SST has a significant warming trend in observations and models (Fig. 5). It  
360 is slightly underestimated in models ( $+0.2^{\circ}$  C/decade) compared to the observations  
361 ( $+0.27^{\circ}$  C/decade). In the observations, it is larger in the ThSOW ( $+0.32^{\circ}$  C/decade) than in the  
362 TiMCW ( $+0.23^{\circ}$  C/decade). These trends are in the range of previous estimates for the same period  
363 in the region, that is [ $+0.2^{\circ}$  C/decade  $+0.5^{\circ}$  C/decade] for observed SST (Cannaby and Hüsrevoglu,  
364 2009, Michel et al., 2009, Smyth et al., 2010, Saulquin and Gohin, 2010, Holt et al., 2012) and  
365 [ $+0.175^{\circ}$  C/decade  $+0.3^{\circ}$  C/decade] for modelled SST (Michel et al., 2009, Holt et al., 2012). The  
366 underestimation of the SST trend in models compared to satellite data has also been observed by  
367 Michel et al. (2009) in a regional modelling study of the Bay of Biscay, in spite of the higher resolution  
368 of their simulation (about 20 km). Their SST trend is of  $+0.22^{\circ}$  C/decade in the model versus  
369  $+0.37^{\circ}$  C/decade in satellite data, over a domain ranging up to  $15^{\circ}$  W into the open ocean.

370 In the observations, the SST trend is concentrated in the autumn season ( $+0.41^{\circ}$  C/decade). The  
371 other indices do not show significant trend. In ThSOW, the date of the autumn onset is also delayed  
372 by 4 day/decade, certainly related to the strong autumn temperature increase of  $+0.48^{\circ}$  C/decade.

373 The warming is there also fairly strong in spring ( $+0.3^{\circ}$  C/decade).

374 CMIP5 models show a significant increase of the annual maximum ( $+0.31^{\circ}$  C/decade), higher than  
375 that of the annual minimum ( $+0.19^{\circ}$  C/decade), resulting in an increase of the annual SST amplitude.  
376 The annual maximum increase is not detected in the time series of indice I3 absolute value (Fig. 5, left  
377 column) because of the large inter-model dispersion for summer temperatures. There is no significant  
378 or a too weak trend in the time series of indices I5 to I8 (Fig. 6), that characterize a possible seasonal  
379 shift. Indeed, models present a constant warming over all seasons of about  $+0.21^{\circ}$  C/decade, with no  
380 significant seasonal shift.

### 381 3.2.3 Natural climate variability versus anthropogenic climate change

382 In Western European marine systems, it is important to take into account the combined effects of  
383 natural climate variability and anthropogenic climate change to conclude on warming trends related to  
384 climate change. Nevertheless, whereas it is clear that there is a significant multidecadal pattern in the  
385 SST, there is still much uncertainty about how to determine the relative contribution of these two  
386 factors to the recent observed warming (Knight et al., 2005, Cannaby and Hüsrevoğlu, 2009, Swanson  
387 et al., 2009, Ting et al., 2009). In our study, trends are computed over a relatively short period (28  
388 years in the observations) compared to the 60 years cycle of the Atlantic Multi-decadal Oscillation  
389 (AMO) natural variability pattern observed over the North Atlantic (Knight et al., 2005). The latter is  
390 characterized by a SST increase over 1980–2007, followed by a decrease up to 2013. Cannaby and  
391 Hüsrevoğlu (2009) have shown that under the AMO warming phase, the AMO variability is responsible  
392 for 50% of the warming trend on the northwestern European coast. If a too short period is considered,  
393 the trend should rather be attributable to AMO natural variability than to anthropogenic climate  
394 change, as in Tréguer et al. (2014), wherein a not really significant slightly negative trend was  
395 estimated over the period 1998–2012 in the coastal area of Iroise Sea. Saulquin and Gohin (2010),  
396 using the same AVHRR–SST satellite data as this study over the period 1986–2006, found identical  
397 spatial distribution of the SST trend with slightly larger values of  $+0.4^{\circ}$  C/decade in TiMCW to  
398  $+0.5^{\circ}$  C/decade in ThSOW. As the period we consider extends up to 2013 and thus contains both a

399 warming and a cooling phase of the AMO natural variability cycle, it explains the slight trend  
400 overestimation in Saulquin and Gohin (2010) and gives more confidence to the trend values of our  
401 study as being for a major part attributable to anthropogenic climate change.

#### 402 3.2.4 Conclusion on SST trends in the Iroise Sea over the previous decades

403 In the off-shore area of the Iroise Sea, the observed mean seasonal cycle of the SST is well  
404 simulated by the CMIP5 multi-model ensemble (Section 3.1). Over the last 30 years, the annual mean  
405 warming is slightly underestimated in models, with an evenly distribution throughout the year and no  
406 seasonal shift; whereas observations show a seasonal shift due to a strong autumn warming, less  
407 noticeable in the rest of the year (Section 3.2).

408 Despite these slight differences, it is appropriate to use the CMIP5 multi-model median derived  
409 from the 5th IPCC future scenarios projections to evaluate the future SST evolution in the Iroise Sea.

#### 410 3.3 Future scenarios

411 In this Section, future changes of SST seasonal cycle in the off-shore area of the Iroise Sea  
412 are estimated from the projections carried out in CMIP5 for the scenarios established in the 5th IPCC  
413 report (IPCC, 2014). Figure 8 (resp. 9) shows time series of indices I1 to I4 (resp. seasonal indices I10  
414 to I13) for the 13 CMIP5 multi-model ensemble median, over 1980–2004 for historical simulations and  
415 2005–2100 for the scenarios RCP2.6, RCP4.5 and RCP8.5 (described in Section 2.1). Anomalies of  
416 indices relative to the time-mean over 1986–2004 are plotted, as in the left column of Figures 5 to 7.  
417 Fits to second order polynomial functions are superimposed.

418 We note an increase of the SST annual mean of  $0.5^{\circ}$  C for the RCP2.6 scenario to  $2.5^{\circ}$  C  
419 for the RCP8.5 one in year 2100. The uncertainty linked to the scenarios, of about  $1.5^{\circ}$  C for the  
420 winter minimum, is half that of the summer maximum. In the scenario RCP2.6, the annual mean and  
421 summer SST increase up to around 2060 and then decline. It is consistent with the radiative forcing  
422 evolution (Van Vuuren et al., 2011), but with a time-lag of 10 to 20 years. In year 2100, seasonal  
423 means converge to a constant warming all year round of  $+0.5^{\circ}$  C. In the scenario RCP4.5, we note an

424 increase followed by a stabilization of the SST around year 2080, again with a time-lag of 10 to 20  
425 years with respect to the imposed radiative forcing. At year 2100, the annual mean is forecast to reach  
426  $+1^{\circ}\text{C}$  with a seasonal range of [ $+0.8^{\circ}\text{C}$   $+1.5^{\circ}\text{C}$ ]. In the scenario RCP8.5, a high rate of surface  
427 temperature increase follows the radiative forcing, reaching  $+2.5^{\circ}\text{C}$  for the annual mean with a  
428 seasonal range of [ $+2^{\circ}\text{C}$   $+3.5^{\circ}\text{C}$ ] in year 2100.

429 For all scenarios, the warming is more moderate in winter-spring and stronger in summer-  
430 autumn (Fig. 9). The warming difference between winter and summer is also highlighted in regional  
431 downscaled projections over the North Sea (Adlandsvik, 2008), the western European continental shelf  
432 (Holt et al., 2010) and the Irish Sea (Olbert et al., 2012). Holt et al. (2010), analyzing the SST and  
433 hydrography changes by the end of the century in a downscaling study including our study region,  
434 associated the SST changes to increasing summer stratification. From a regional perspective, a  
435 comparison between our results and that of the latter study is interesting, although somewhat tricky  
436 because different scenarios are simulated. In scenario SRES-A1B, Holt et al. (2010) simulate an  
437 increase of the Iroise Sea SST of about  $+2.5^{\circ}\text{C}$  in winter to  $+3.5^{\circ}\text{C}$  in autumn. The scenario SRES-  
438 A1B is close to the scenario RCP6.0, with a radiative forcing increase between scenarios RCP4.5 and  
439 RCP8.5. In our study, the range between scenarios RCP4.5 and RCP8.5 gives an increase of [ $+0.8^{\circ}\text{C}$   
440  $+2^{\circ}\text{C}$ ] in winter to [ $+1.3^{\circ}\text{C}$   $+3^{\circ}\text{C}$ ] in summer. Thus, the warming on the shelf seems  
441 underestimated in global climate models, especially in summer-autumn, due to a poor simulation of  
442 physical and hydrographical processes specific to the oceanic shelves in Brittany.

443 To go further in the analysis, we now focus on future changes in SST interannual variability  
444 and extremes. Indeed, climate change is likely to be associated with an increase of the occurrence of  
445 extreme events (IPCC, 2014), linked to a modification of the statistical distribution of the climate  
446 variables. Changes in the shape of the probability distribution of SST may contribute as much to  
447 changes in extremes as a shift of mean temperatures (Schaeffer et al., 2005). To evaluate the changes  
448 in mean seasonal SST extremes, the probability distribution functions (PDF) of the winter and summer  
449 mean SST in CMIP5 multi-model ensemble are represented in Figure 10 for the present-day climate

450 (1986–04), the near–future (2031–50) and the far–future (2081–2100) climates. Changes in inter–model  
451 variability are negligible compared to changes in interannual variability (not shown). In the near–future,  
452 a similar increase of SST characteristics (mean and variance) is simulated in all three scenarios for both  
453 seasons. In the far–future, the SST variance increases in the three scenarios, associated with an  
454 additional increase in the mean SST in scenarios RCP4.5 and RCP8.5. The increase of the mean SST is  
455 correlated with an increase of its variance and tail and thus of the probability in the occurrence of  
456 extreme temperatures. In all periods, the variance of the SST is larger in summer than in winter. All  
457 these projected changes in the SST mean seasonal cycle and interannual variability, more intense in  
458 summer, may impact critically marine ecosystems.

#### 459 4. Conclusion

460 In this study, previous and projected SST seasonal changes have been estimated in the Iroise Sea  
461 from satellite data and CMIP5 multi–model ensemble. To this end, a set of indices has been developed  
462 to characterize the change of SST, focusing particularly on the seasonal cycle and its modification.  
463 Here, the benefit of these indices to estimate warming trends in the SST seasonal cycle is highlighted  
464 in the Iroise Sea. This new approach can be applied to any ocean region of the world.

465 We first evaluated SST seasonal changes in the previous decades within the study area, using  
466 high–resolution satellite observations. In the Iroise Sea, a significant warming trend is concentrated in  
467 the autumn season. It is not significant in summer, albeit visible in the observations, because of the  
468 large interannual variability during this season. The autumn trend is stronger offshore, with a SST  
469 annual mean increase of  $0.32^{\circ}$  C/decade, but weaker in coastal waters ( $0.23^{\circ}$  C/decade), where a  
470 strong vertical mixing induced by tides and winds acts to reduce surface warming. Then, the  
471 performance of an ensemble of CMIP5 climate models in simulating recent seasonal changes of SST in  
472 the region is estimated. Because of their low resolution, CMIP5 global simulations are rarely used to  
473 evaluate SST changes at regional scale. Yet, our study highlights they may provide a first order  
474 estimate of SST seasonal cycle climatology under present and future climate conditions. Indeed, the  
475 median of CMIP5 models reproduces very well the observed SST mean seasonal cycle in off–shore

476 waters. It is less proficient in regions closer to the coast, due to model coarse resolution and the  
477 absence of tidal processes. The trend of the annual mean SST is relatively well simulated, albeit  
478 somewhat underestimated ( $0.20^{\circ}$  C/decade) and evenly distributed throughout the year. This  
479 assessment of CMIP5 models skill to reproduce the observed recent SST changes gives confidence in  
480 future change estimates from CMIP5 models simulations in the off-shore seas of the Western English  
481 Channel.

482 In this study, estimate of SST future warming related to anthropogenic climate is given for the  
483 Iroise Sea, where the annual mean SST increase ranges from  $0.5^{\circ}$  C (RCP2.6) to  $2.5^{\circ}$  C (RCP8.5) by  
484 year 2100, with a seasonal modulation leading to a more intense warming in summer–autumn than in  
485 winter–spring. The simulated future evolution of the SST trend, with larger values in summer–autumn  
486 than in winter–spring is consistent with seasonal variations of the observed trend in the previous  
487 decades. The increase of the mean SST is correlated to an increase of its variance and interannual  
488 variability and thus of the probability in the occurrence of extreme temperatures, mostly in summer.

489 Nevertheless, in this region, significant differences have been highlighted in the previous decades  
490 from satellite observations in the warming intensity and seasonal distribution between ThSOW, located  
491 offshore from the Ushant front, and TiMCW. In the ThSOW, the observed warming trend is  
492  $+0.32^{\circ}$  C/decade over the last 30 years, while it is  $+0.23^{\circ}$  C/decade in the TiMCW. Nevertheless,  
493 due to their poor resolution (among other factors), CMIP5 global climate models cannot simulate SST  
494 changes in coastal areas of the Iroise Sea. Thus, we highlight the need to refine resolution in the ocean  
495 and to include tides to better simulate the mesoscale dynamics and changes. An increase of seasonal  
496 variability due to marine downscaling was observed in Adlandsvik (2008), but with a regional ocean  
497 model covering only the North Sea. Higher resolution in the atmosphere may also improve the realism  
498 of the simulations, as demonstrated by Muller et al. (2007) in a high-resolution ( $\sim 6$  km) simulation of  
499 the Iroise Sea with the regional ocean model MARS, forced by atmospheric fields downscaled at the  
500 same resolution. They shown that a better constrained and higher resolution atmospheric forcing  
501 improves coastal winds, but also hydrography and oceanic circulation in the Iroise Sea. Then, to go

502 further and address the issue of uncertainty, an ensemble of coupled ocean-atmosphere regional  
503 simulations could be performed over the northwestern European continental shelf, driven by a set of  
504 CMIP5 global climate model under historical conditions and then RCP scenarios to cover the period  
505 1980–2100.

506       Regarding environmental impacts in the Western English Channel, the predicted increase in SST  
507 may strongly affect marine biology, particularly algae biomass and phenology. Increase in temperature  
508 may be responsible for more frequent occurrences of Harmful Algal Blooms (HAB) in the Western  
509 English Channel waters. Using a modelling approach associating the IPSL-CM4 global climate model  
510 future projection under the SRES-A1B scenario and the regional oceanographic-biogeochemical model  
511 POLCOMS-ERSEM over the Northwestern European shelf, Glibert et al. (2014) have projected an  
512 expansion in area and number of months annually conducive to development of pelagic *Prorocentrum*  
513 and *Karenia* HABs along the Northwestern European Shelf system by 2100. Moreover, a possible shift  
514 of the thermal front where this species thrives towards shallower waters would have more dramatic  
515 effects on the benthic fauna, including exploited shellfish (e.g. oysters, scallops).

516       The impacts of the SST increase on the evolution of the kelp forest in Northern Brittany have  
517 been highlighted by Meleder et al. (2010), going to a possible complete extinction in the area. The  
518 distribution of kelp *Laminaria digitata* ranges from the Southern Brittany to Norway with an optimum  
519 range of temperature between 10° C and 15° C and a reproduction impaired above 18° C. Raybaud  
520 et al. (2013) show that *Laminaria digitata* could disappear from the coast of France as early as the  
521 2050s, using MPI-ESM-LR and CNRM-CM5 CMIP5 models and three RCP scenarios (RCP2.6,  
522 RCP4.5 and RCP8.5). It is likely that a delay will be observed in the mixed coastal waters of Northern  
523 Brittany, that are not explicitly represented in the latter global climate models. In these coastal  
524 waters, we expect a slower increase in temperature. Changes in *Laminaria digitata* and more  
525 importantly the forest-forming *Laminaria hyperboles* (Smale et al., 2013) would have profound  
526 consequences for the ecosystems of the English Channel and Southern North Sea ; although some  
527 replacement would occur from the warm-water species *Laminaria ochroleuca*.

528 More generally, studies on changes in the distribution of species in response to climate  
529 fluctuations like the AMO (Mieszkowska et al., 2014) and climate change (Southward et al 1995;  
530 Herbert et al 2003 ; Hawkins et al 2008 ; Philippart et al., 2011) in the Channel region have mainly  
531 shown advance of Southern species. Interestingly, many Northern species seem to refuge around  
532 Brittany and Cornwall, in cold water refuges as those shown on Figure 1. The large tidal range areas in  
533 East Brittany/Normandy and around the Channel Islands provide refuges for cold water species, also  
534 because of the equally distribution of heat between bottom and surface waters leading to a similar  
535 warming of all the water column. This migration of the species has implications for fisheries. Genner et  
536 al. (2004, 2010) shows that climate change and particularly sea surface temperature change has  
537 dramatic effects on marine fish community composition and abundance, especially for small species less  
538 impacted by overharvesting. Going back to the Middle Ages, Southward et al. (1988) demonstrate the  
539 impact of sea temperature on fluctuations in herring and pilchard fisheries.

540

541

#### 542 *Acknowledgments*

543 This work has been funded by the Belmont Forum International Opportunity Fund, in the  
544 framework of the project ARTISTICCC (Adaptation Research a Transdisciplinary Community and Policy  
545 Centred Approach). We acknowledge the World Climate Research Program's Working Group on  
546 Coupled Modelling, which is responsible for CMIP, and we thank the climate modeling groups (listed in  
547 Table 1 of this paper) for producing and making available their model output. For CMIP the U.S.  
548 Department of Energy's Program for Climate Model Diagnosis and Intercomparison provides  
549 coordinating support and led development of software infrastructure in partnership with the Global  
550 Organization for Earth System Science Portals. We acknowledge Ifremer for providing its satellite-  
551 derived SST data set; the Met Office for the OSTIA data set and MyOcean for the ODYSSEA data set.

## 552 **List of tables and figures**

553 **Tab. 1** CMIP5 climate models used in the study. Name, resolution of the ocean model, and  
554 characteristics of its horizontal grid around Brittany.

555 **Tab. 2** Presentation of indices. Characteristics, number, definition, computing methodology.

556 **Fig. 1** Snapshot of the SST on 18th June 2003 from Ifremer satellite-derived data. Selected  
557 ThSOW and TiMCW areas in the Iroise Sea, the English Channel and the Bay of Biscay (solid line). A  
558 typical grid cell size for CMIP5 models (dashed line), representative of the grid cell size of 10 models  
559 over the 13 models of the study.

560 **Fig. 2** Mean annual cycle of SST: ensemble median (solid) and mean (dashed) of 13 CMIP5 models  
561 (black) as well as satellite data spatial mean over ThSOW (green) and TiMCW (red), averaged over  
562 1980–04 for CMIP5 and 1986–13 for satellite data. The shading indicates the interquartile ensemble  
563 spread (range between the 25th and 75th quantiles).

564 **Fig. 3** The “portrait” diagram of relative errors in the 1986–2004 climatologies of SST indices in  
565 Iroise Sea simulated by the CMIP5 models with respect to the satellite data: (a) TiMCW and (b)  
566 ThSOW.

567 **Fig. 4** Time series of monthly mean SST from 1980 to 2013 of the CMIP5 median (black), spatial  
568 mean of satellite data over ThSOW (green) and TiMCW (red) in the Iroise Sea, the English channel  
569 and the Bay of Biscay. The shading indicates the interquartile ensemble spread (range between the  
570 25th and 75th quantiles). Trends statistically significant at 95% confidence level are superimposed.

571 **Fig. 5** I1 to I4 SST indices in the Iroise Sea from 1980 to 2013. For the respective index, the left  
572 column displays absolute values of the CMIP5 median (bold black) and of the spatial mean of the  
573 satellite data (grey) over the Iroise Sea, with their associated trends. The satellite data average over  
574 the ThSOW (green) and TiMCW (red) are superimposed in dashed line. The right column shows  
575 anomalies with respect to the common period 1986–2004 of the CMIP5 median (black) and of satellite  
576 data spatial mean over ThSOW (green) and TiMCW (red). The shading indicates the interquartile

2:

577 ensemble spread of CMIP5 models (range between the 25th and 75th quantiles). Trends statistically  
578 significant at 95% confidence level are superimposed.

579 **Fig. 6** I5 to I9 SST indices in the Iroise Sea from 1980 to 2013. For the respective index, the left  
580 column displays absolute values of the CMIP5 median (bold black) and of the spatial mean of the  
581 satellite data (grey) over the Iroise Sea, with their associated trends. The satellite data average over  
582 the ThSOW (green) and TiMCW (red) are superimposed in dashed line. The right column shows  
583 anomalies with respect to the common period 1986–2004 of the CMIP5 median (black) and of satellite  
584 data spatial mean over ThSOW (green) and TiMCW (red). The shading indicates the interquartile  
585 ensemble spread of CMIP5 models (range between the 25th and 75th quantiles). Trends statistically  
586 significant at 95% confidence level are superimposed.

587 **Fig. 7** I10 to I13 SST indices in the Iroise Sea from 1980 to 2013. For the respective index, the  
588 left column displays absolute values of the CMIP5 median (bold black) and of the spatial mean of the  
589 satellite data (grey) over the Iroise Sea, with their associated trends. The satellite data average over  
590 the ThSOW (green) and TiMCW (red) are superimposed in dashed line. The right column shows  
591 anomalies with respect to the common period 1986–2004 of the CMIP5 median (black) and of satellite  
592 data spatial mean over ThSOW (green) and TiMCW (red). The shading indicates the interquartile  
593 ensemble spread of CMIP5 models (range between the 25th and 75th quantiles). Trends statistically  
594 significant at 95% confidence level are superimposed.

595 **Fig. 8** I1 to I4 SST indices in the Iroise Sea: for the median of the historical CMIP5 simulations  
596 during 1980–2004 (black), for satellite data spatial mean over ThSOW during 1986–2013 (grey), for  
597 the median of the CMIP5 future projections over 2005–2100 in the RCP2.6 (green; scenario designed  
598 to meet the 2° C global average warming target compared to pre-industrial conditions by 2100),  
599 RCP4.5 (red; where radiative forcing peaks at about 4.5 W/m<sup>2</sup> in year 2100) and RCP8.5 (blue;  
600 assuming a high rate of radiative forcing increase, peaking at 8.5 W/m<sup>2</sup> in year 2100) scenarios. The  
601 shading indicates the interquartile ensemble spread (range between the 25th and 75th quantiles).  
602 Indice anomalies relative to the time-mean over 1986–2004 are plotted. Fits to second order

603 polynomial functions are superimposed.

604 **Fig. 9** I10 to I13 SST indices in the Iroise Sea: for the median of the historical CMIP5 simulations  
605 during 1980–2004 (black), for satellite data spatial mean over ThSOW during 1986–2013 (grey), for  
606 the median of the CMIP5 future projections over 2005–2100 in the RCP2.6 (green; scenario designed  
607 to meet the 2° C global average warming target compared to pre-industrial conditions by 2100),  
608 RCP4.5 (red; where radiative forcing peaks at about 4.5 W/m<sup>2</sup> in year 2100) and RCP8.5 (blue;  
609 assuming a high rate of radiative forcing increase, peaking at 8.5 W/m<sup>2</sup> in year 2100) scenarios. The  
610 shading indicates the interquartile ensemble spread (range between the 25th and 75th quantiles).  
611 Indices anomalies relative to the time-mean over 1986–2004 are plotted. Fits to second order  
612 polynomial functions are superimposed.

613 **Fig. 10** Probability distribution function (pdf) of the winter (top panels) and summer (bottom  
614 panels) means over 1986–2004 for CMIP5 historical simulations (black), for satellite data spatial mean  
615 in the Iroise Sea ThSOW (grey); and over 2031–2050 (left panels) and 2081–2100 (right panels) for  
616 CMIP5 future projections in the RCP2.6 (green), RCP4.5 (red) and RCP8.5 (blue) scenarios.

617 **References**

618 Ådlandsvik B. 2008. Marine Downscaling of a Future Climate Scenario for the North Sea. *Tellus*  
619 **60A**:451-458.

620 Altizer S, Ostfeld RS, Johnson PTJ, Kutz S and Harvel CD. 2013. Climate change and infectious  
621 diseases: from evidence to a predictive framework. *Science* **341**: 514-519.

622 Autret E, Piolle J-F. 2011. Product User Manual for ODYSSEA Level 3 and 4 Global and Regional  
623 Products. MYO-PUM-SST-TAC-ODYSSEA, Ifremer/CERSAT.

624 Bellard C, Bertelsmeier C, Leadley P, Thuiller W and Courchamp F. 2012. Impacts of climate  
625 change on the future of biodiversity. *Ecology Letters* **15**: 365-377.

626 Bissinger JE, Montagnes DJS, Sharples J, Atkinson D. 2008. Predicting marine phytoplankton  
627 maximum growth rates from temperature: improving on the Eppley curve using quantile regression.  
628 *Limnology and Oceanography* **53 (2)** :487-493.

629 Cambon G. 2008. Étude numérique de la mer d'Iroise: Dynamique, variabilité du front d'Ouessant  
630 et évaluation des échanges cross-frontaux. Ph.D. thesis, Univ. de Bretagne Occident., Brest, France.

631 Cannaby H and Hüsrevoğlu YS. 2009. The influence of low-frequency variability and long-term  
632 trends in North Atlantic sea surface temperature on Irish waters. *ICES Journal of Marine Science* **66**:  
633 1480-1489.

634 Chelton DB and SP Xie. 2010. Coupled ocean-atmosphere interaction at oceanic mesoscales.  
635 *Oceanography Magazine*, **23**:52-69.

636 Chen B .2015. Patterns of thermal limits of phytoplankton. *Journal of Plankton Research*,  
637 doi :10.1093/plankt/fbv009.

638 Collins WJ et al. 2011. Development and evaluation of an Earth-System model HadGEM2.  
639 *Geosci. Model Dev.*, 4, 1051-1075, doi:10.5194/gmd-4-1051-2011.

640 Dong BW, Sutton RT. 2005. Mechanism of interdecadal thermohaline circulation variability in a

- 641 coupled ocean-atmosphere GCM. *J. Clim*, **18** :1117-1135.
- 642 Donlon CJ, Martin M, Stark JD, Roberts-Jones J, Fiedler E, Wimmer W. 2011. The operational  
643 sea surface temperature and sea ice analysis (OSTIA) system. *Rem. Sens. Environ.*,  
644 <http://dx.doi.org/10.1016/j.rse.2010.10.017>.
- 645 Dye SR, Hughes SL, Tinker J, Berry DI, Holliday NP, Kent EC, Kennington K, Inall M, Smyth T,  
646 Nolan G, Lyons K, Andres O and Beszczynska-Möller A. 2013. Impacts of climate change on  
647 temperature (air and sea). *MCCIP Science Review* 2013, 1-12. doi:10.14465/2013.arc01.001-012.
- 648 Eliseev AV and II Mokhov. 2003. Amplitude-Phase characteristics of the Annual cycle of Surface  
649 Air Temperature in the Northern Hemisphere. *Advances in Atm. Sciences* **20**:1-16.
- 650 Esnaola G, Sáenz J, Zorita E, Lazure P, Ganzedo U, Fontán A, Ibarra-Berastegi G and A Ezcurra.  
651 2012. Coupled air-sea interaction patterns and surface heat-flux feedback in the Bay of Biscay. *J.*  
652 *Geophys. Res.* **117**:C06030, doi:10.1029/2011JC007692.
- 653 Foley AM. 2010. Uncertainty in regional climate modelling: A review. *Progress in Physical*  
654 *Geography*. doi: 10.1177/0309133310375654.
- 655 Friocourt YF, Skogen MD, Stolte W and Albretsen J. 2012. Marine downscaling of a future climate  
656 scenario in the North Sea and possible effects on dinoflagellate harmful algal blooms. *Food Additives &*  
657 *Contaminants: Part A*, 29:1630-1646. doi:10.1080/19440049.2012.714079.
- 658 Genner MJ, Sims DW et al. 2004. Regional climatic warming drives long-term community changes of  
659 British marine fish. *Proc R Soc B*, 271: 655-61.
- 660 Genner MJ, Sims DW, Southward AJ, Budd GC, Masterson P, Mchugh M, Rendle P, Southall EJ,  
661 Wearmouth VJ, Hawkins SJ. 2010. Body size-dependent responses of a marine fish assemblage to climate  
662 change and fishing over a century-long scale. *Global Change Biology*, 16(2): 517-527,  
663 DOI: 10.1111/j.1365-2486.2009.02027.x.
- 664 Gleckler PJ, KE Taylor, and C Doutriaux. 2008. Performance metrics for climate models. *J.*

- 665 *Geophys. Res.* **113**:2156–2202, DOI: 10.1029/2007JD008972.
- 666 Glibert P M, JI Allen, Y Artioli, A Beusen, L Bouwman, J Harle, R Holmes and J Holt .2014.  
667 Vulnerability of coastal ecosystems to changes in harmful algal bloom distribution in response to  
668 climate change: projections based on model analysis. *Global Change Biology* **20(12)**:3845–58. doi:  
669 10.1111/gcb.12662.
- 670 Gohin F, P Bryère, J Griffiths. 2015. The exceptional surface turbidity of the North–West  
671 European shelf seas during the stormy 2013–2014 winter: consequences for the initiation of the  
672 phytoplankton blooms? *Journal of Marine Systems*. **148**:70–85. doi:10.1016/j.jmarsys.2015.02.001.
- 673 Gordon C, Cooper C, Senior A, Banks H, Gregory JM, Johns TC, Mitchell J, Wood R. 2000. The  
674 simulation of SST, sea ice extent and ocean heat transports in a version of the Hadley Centre coupled  
675 model without flux adjustments. *Climate Dynamics* **16** : 147–168. doi:10.1007/s003820050010.
- 676 Gröger M, E Maier–Reimer, U Mikolajewicz, A Moll and D Sein. 2013. NW European shelf under  
677 climate warming: implications for open ocean - shelf exchange, primary production, and carbon  
678 absorption. *Biogeosciences* **10**:3767–3792, doi:10.5194/bg-10-3767-2013.
- 679 Hartman SE, Hartman MC, Hydes DJ, Smythe–Wright D, Gohin F, Lazure P. 2014. The role of  
680 hydrographic parameters, measured from a ship of opportunity, in bloom formation of *Karenia*  
681 *mikimotoi* in the English Channel. *Journal of Marine Systems* **140**:39–49,  
682 doi:10.1016/j.jmarsys.2014.07.001.
- 683 Hawkins SJ, Southward AJ, Genner MJ 2003. Detection of environmental change in a marine  
684 ecosystem – evidence from the western English Channel. *Sci Total Environ* **310**: 245–256.
- 685 Hawkins SJ, Moore P, Burrows M, Poloczanska E, Mieszkowska N, Jenkins SR, Thompson RC,  
686 Genner MJ & Southward AJ 2008. Complex interactions in a rapidly changing world: responses of  
687 rocky shore communities to recent climate change, *Climate Research*, **37**:123 – 133.
- 688 Hawkins E, Sutton R. 2009. The potential to narrow uncertainty in regional climate predictions.  
689 *Bull. Am. Meteorol. Soc.* **90**:1095–1107. doi:10.1175/2009BAMS2607.1

690 Herbert RJ, Hawkins SJ, Sheader M and Southward AJ 2003. Range extension and reproduction of  
691 the barnacle *Balanus perforatus* in the eastern English Channel. *Journal of the Marine Biological*  
692 *Association of the United Kingdom*, **83(1)**: 73–82.

693 Helmuth B, Broitman BR, Blanchette CA, Gilman S, Halpin P, Harley C, O'Donnell MJ, Hofmann  
694 GE, Menge B, Strickland D 2006. Mosaic patterns of thermal stress in the rocky intertidal zone:  
695 implications for climate change. *Ecological monographs* **76(4)**: 461–479.

696 Hemery G, D'Amico F, Castege I, Dupont B, D'Elbée J, Lalanne Y, Mouches C. 2008. Detecting  
697 the impact of oceano-climatic changes on marine ecosystems using a multivariate index : the case of  
698 the Bay of Biscay (North Atlantic-European Ocean). *Global Change Biology* **14 (1)**:27–38. DOI :  
699 10.1111/j.1365-2486.2007.01471.x

700 Hjollo S, MD Skogen, E Svendsen. 2009. Exploring currents and heat within the North Sea using a  
701 numerical model. *Journal of Marine Systems* **78(1)**:180–192, DOI: 10.1016/j.jmarsys.2009.06.001.

702 ter Hofstede R, Hiddink JG, Rijnsdorp AD. 2010. Regional warming changes fish species richness  
703 in the eastern North Atlantic Ocean. *Mar. Ecol. Prog. Ser.* **414**:1–9, doi: 10.3354/meps08753.

704 Hogg, A.McC., W.K. Dewar, P. Berloff, S. Kravtsov, and D.K. Hutchinson. 2009. The effects of  
705 mesoscale ocean-atmosphere coupling on the large-scale ocean circulation. *Journal of*  
706 *Climate* **22**:4,066–4,082.

707 Holt J, Harle J, Proctor R, Michel S, Ashworth M, Batstone C, Allen I, Holmes R, Smyth T,  
708 Haines K, Bretherton D, Smith G. 2009. Modelling the global coastal ocean. *Philosophical*  
709 *Transactions of the Royal Society A: Mathematical, Physical and Engineering Sciences* **367**  
710 (1890):939–951. doi:10.1098/rsta.2008.0210.

711 Holt J, S Wakelin, J Lowe and J Tinker. 2010. The potential impacts of climate change on the  
712 hydrography of the northwest European continental shelf. *Progress In Oceanography* **86 (3–4)**:361–  
713 379, doi:10.1016/j.pocean.2010.05.003.

714 Holt J, Hughes S, Hopkins J, Wakelin SL, Holliday ND, Dye S et al. 2012. Multi-decadal

715 variability and trends in the temperature of the northwest European continental shelf: A model-data  
716 synthesis. *Progress in Oceanography* **106**:96–117. doi:10.1016/j.pocean.2012.08.001.

717 Holt J et al. 2014. Challenges in integrative approaches to modelling the marine ecosystems of the  
718 North Atlantic: Physics to Fish and Coasts to Ocean. *Progress in Oceanography*  
719 doi:10.1016/j.pocean.2014.04.024.

720 IPCC. 2007. Climate Change 2007: Synthesis Report. Contribution of Working Groups I, II and III  
721 to the Fourth Assessment Report of the Intergovernmental Panel on Climate Change. Core Writing  
722 Team, Pachauri, R.K. and Reisinger, A. (Eds.) IPCC, Geneva, Switzerland, pp 104.

723 IPCC. 2014. Climate Change 2014: Impacts, Adaptation, and Vulnerability. Part B: Regional  
724 Aspects. Contribution of Working Group II to the Fifth Assessment Report of the Intergovernmental  
725 Panel on Climate Change [Barros, V.R., C.B. Field, D.J. Dokken, M.D. Mastrandrea, K.J. Mach, T.E.  
726 Bilir, M. Chatterjee, K.L. Ebi, Y.O. Estrada, R.C. Genova, B. Girma, E.S. Kissel, A.N. Levy, S.  
727 MacCracken, P.R. Mastrandrea, and L.L. White (eds.)]. Cambridge University Press, Cambridge,  
728 United Kingdom and New York, NY, USA, 688 pp.

729 Karl T, and D Easterling. 1999. Climate extremes: Selected review and future research directions.  
730 *Clim. Chang.* **42**:309-325.

731 Klein Tank AG, FW Zwiers and X Zhang. 2009. Guidelines on analysis of extremes in a changing  
732 climate in support of informed decisions for adaptation. Climate data and monitoring WCDMP–No. 72,  
733 WMO–TD No. 1500, 56 pp.

734 Knight JR, RJ Allan, CK Folland, M Vellinga, and ME Mann. 2005. A signature of persistent  
735 natural thermohaline circulation cycles in observed climate. *Geophys. Res. Lett.* **32**, L20708,  
736 doi:10.1029/2005GL024233.

737 Lazure P, Garnier V, Dumas F, Herry C, Chifflet M. 2009. Development of a hydrodynamic model  
738 of the Bay of Biscay. Validation of hydrology. *Continental Shelf Research* **29(8)**:985–997,  
739 <http://dx.doi.org/10.1016/j.csr.2008.12.017>.

- 740 Le Boyer A, G Cambon, N Danialt, S Herbette, B Le Cann, L Marié and P Morin. 2009.  
741 Observations of the Ushant tidal front in September 2007. *Cont. Shelf Res.* **29**:1026–1037,  
742 doi:10.1016/j.csr.2008.12.020.
- 743 Mariette V, Le Cann B. 1985. Simulation of the formation of Ushant thermal front. *Cont. Shelf*  
744 *Res.* **4 (6)**:637–660.
- 745 Méléder V, Populus J, Guillaumont B, Perrot T and Mouquet P. 2010. Predictive modelling of  
746 seabed habitats – Case study of subtidal kelp forests on the coast of Brittany, France. *Marine Biology*  
747 **157**: 1525–1541. doi:10.1007/s00227-010-1426-4.
- 748 Meyer EM, Pohlmann T and Weisse R .2011. Thermodynamic variability and change in the North  
749 Sea (1948–2007) derived from a multidecadal hindcast. *Journal of Marine Systems* **86(3–4)**:35–44.  
750 doi:10.1016/j.jmarsys.2011.02.001.
- 751 Michel S, Treguier A–M, Vandermeirsch F .2009. Temperature variability in the Bay of Biscay  
752 during the past 40 years, from an in situ analysis and a 3D global simulation. *Continental Shelf*  
753 *Research* **29(8)**:1070–1087. <http://dx.doi.org/10.1016/j.csr.2008.11.019>
- 754 Mieszkowska N, Burrows M, Pannacciulli F and Hawkins SJ. 2014. Multidecadal signals within co-  
755 occurring intertidal barnacles *Semibalanus balanoides* and *Chthamalus* spp. linked to the Atlantic  
756 Multidecadal Oscillation. *Journal of Marine Systems* **133**: 70–76.
- 757 Millennium Ecosystem Assessment. 2005. Ecosystems and Human Well-being: Synthesis. Island  
758 Press, Washington, DC.
- 759 Moss RH et al. 2010. The next generation of scenarios for climate change research and  
760 assessment. *Nature* **463**:747–756, doi:10.1038/nature08823.
- 761 Muller H, F Dumas, B Blancke and V Mariette. 2007. High-resolution atmospheric forcing for  
762 regional oceanic model: the Iroise Sea. *Ocean Dynamics* **57(4–5)** :375–400, doi :10.1007/s10236-007-  
763 0115-4.
- 764 Nakicenovic N, Swart R. 2000. Special Report on Emissions Scenarios. A Special Report of

765 Working Group III of the Intergovernmental Panel on Climate Change. Cambridge University Press,  
766 Cambridge, UK and New York, NY, USA.

767 Olbert AI, Dabrowski T, Nash S, and Hartnett M. 2012. Regional modelling of the 21st century  
768 climate changes in the Irish Sea. *Cont. Shelf. Res.* **41**:48-60.

769 Philippart CJM, Anadón R, Danovaroc R, Dippnerd JW, Drinkwater KF, Hawkins SJ, Oguz T,  
770 O'Sullivan G, Reid PC 2011. Impacts of climate change on European marine ecosystems: observations,  
771 expectations and indicators. *J. Exp. Mar. Biol. Ecol.*, 400.

772 Pingree RD and DK Griffiths .1978. Tidal fronts on the shelf seas around the British Isles. *J.*  
773 *Geophys. Res.* **83**:4615-4622

774 Poloczanska ES, Hawkins SJ, Southward AJ and Burrows MT 2008. Modeling the response of  
775 populations of competing species to climate change. *Ecology*, **89(11)**: 3138-3149.

776 Raybaud V, G Beaugrand, E Goberville, G Delebecq, C Destombe, M Valero et al. 2013. Decline  
777 in Kelp in West Europe and Climate. *PLoS ONE* **8(6)**. doi:10.1371/journal.pone.0066044

778 Rhein M et al. 2013. Observations: Ocean (Chapter 3). In: Climate Change 2013: The Physical  
779 Science Basis. Contribution of Working Group I to the Fifth Assessment Report of the  
780 Intergovernmental Panel on Climate Change [Stocker, T. (eds.)]. Cambridge University Press,  
781 Cambridge, United Kingdom and New-York, NY, USA, 255-315.  
782 doi:10.1017/CBO9781107415324.010.

783 Riahi K, Krey V, Rao S, Chirkov V, Fischer G, Kolp P, Kindermann G, Nakicenovic N, Rafai P  
784 .2011. RCP-8.5: Exploring the consequence of high emission trajectories. *Climatic Change* **109**, Issue  
785 1-2, doi:10.1007/s10584-011-0149-y.

786 Saulquin B, Gohin F .2010. Mean seasonal cycle and evolution of the sea surface temperature from  
787 satellite and in situ data in the English Channel for the period 1986-2006. *Int. J. Remot. Sens.* **31**:  
788 4069-4093.

789 Schrum C. 2001. Regionalization of climate change for the North Sea and the Baltic Sea. *Climate*  
3:

- 790 *Research* **18**:31-37.
- 791 Sharples J, Holt J and Dye SR. 2013. Impacts of climate change on shelf sea stratification. *MCCIP*  
792 *Science Review 2013* 67-70, doi:10.14465/2013.arc08.067-070.
- 793 Sillmann J, VV Kharin, X Zhang, FW Zwiers, and D Bronaugh. 2013. Climate extremes indices in  
794 the CMIP5 multi-model ensemble: Part 1. Model evaluation in the present climate. *J. Geophys. Res.*  
795 *Atmos.* **118**:1716-1733, doi:10.1002/jgrd.50203.
- 796 Simpson JH, CM Allen and NC Morris. 1978. Fronts on the continental shelf. *J. Geophys. Res.*  
797 **83(C9)**:4607-4614.
- 798 Smale DA, Burrows M, Moore P, O'Connor N and Hawkins S. 2013. Threats and knowledge gaps  
799 for ecosystem services provided by kelp forests: a northeast Atlantic perspective. *Ecology and*  
800 *Evolution*, **3**: 4016-4038.
- 801 Smyth TJ, JR Fishwick, L Al-Moosawi, DG Cummings, C Harris, V Kitidis, A Rees, V Martinez-  
802 Vicente and E Woodward. 2010. A broad spatio-temporal view of the Western English Channel  
803 Observatory. *J. Plankton Res.* **32 (5)**: 585-601. doi: 10.1093/plankt/fbp128.
- 804 Southward AJ. 1980. The western English Channel - an inconstant ecosystem? *Nature*, **285**: 361-  
805 366, doi:10.1038/285361a0.
- 806 Southward AJ, Boalch GT, Maddock L. 1988. Fluctuations in the herring and pilchard fisheries of  
807 Devon and Cornwall linked to change in climate since the 16th century. *J Mar Biol Ass*, 68: 423-445.
- 808 Southward AJ, SJ Hawkins and MT Burrows. 1995. 70 years observations of changes in  
809 distribution and abundance of zooplankton and intertidal organisms in the western English Channel in  
810 relation to rising sea temperature. *Journal of Thermal Biology*, **20**: 127-155.
- 811 Southward AJ, Langmead O, Hardman-Mountford NJ, Aiken J et al. 2005. Long-term  
812 oceanographic and ecological research in the Western English Channel. *Adv Mar Biol* **47**:1-105.
- 813 Swanson KL, G Sugihara, AA Tsonis. 2009. Long-term natural variability and 20th century

- 814 climate change. *Proceedings of the National Academy of Sciences of the United States of America*.  
815 **106**:16120–16123.
- 816 Taylor KE, RJ Stouffer and GA Meehl. 2012. An overview of CMIP5 and the experiment design.  
817 *Bull. Am. Meteorol. Soc.* **93(4)**:485–498, doi:10.1175/BAMS-D-11-00094.1.
- 818 Thomas Y, S Pouvreau, M Alunno-Bruscia, L Barillé, F Gohin, P Bryère, P Gernez. 2016. Global  
819 change and climate-driven invasion of the Pacific Oyster (*Crassostrea gigas*) along European coasts: a  
820 bioenergetics modelling approach. *Journal of Biogeography* **43**:568–579.
- 821 Thomson AM, Calvin KV, Smith SJ, Kyle GP, Volke A, Patel P, Delgado-Arias S, Bond-Lamberty  
822 B, Wise MA, Clarke LE, Edmonds JA. 2011. RCP4.5: A pathway for stabilization of radiative forcing  
823 by 2100. *Climatic Change* **109**, Issue 1–2, doi:10.1007/s10584-011-0151-4.
- 824 Ting M, Kushnir Y, Seager R, Li C. 2009. Forced and internal twentieth-century SST trends in  
825 the North Atlantic. *J. Climate* **22**:1469–81, DOI: 10.1175/2008JCLI2561.1.
- 826 Treguer P, E Goberville, N Barrier, S L’Helguen, P Morin, Y Bozec, P Rimmelin-Maury, M  
827 Czamanski, E Grossteffan, T Cariou, M Repecaud, L Quemener . 2014. Large and local-scale  
828 influences on physical and chemical characteristics of coastal waters of Western Europe during winter.  
829 *Journal of Marine Systems* **139**: 79–90. <http://dx.doi.org/10.1016/j.jmarsys.2014.05.01>
- 830 Uppala SM et al. 2005. The ERA-40 re-analysis. *Q. J. Roy. Meteor. Soc.* **131**: 2961–3012.
- 831 Vanhoutte-Brunier A, Fernand L, Menesguen A, Lyons S, Gohin F, Cugier P. 2008. Modelling  
832 the *Karenia mikimotoi* bloom that occurred in the western English Channel during summer 2003.  
833 *Ecological Modelling* **210(4)**:351–376. doi:10.1016/j.ecolmodel.2007.08.025
- 834 Van Vuuren DP et al. 2011. The representative concentration pathways: an overview. *Clim.*  
835 *Change* **109**:5–31, doi:10.1007/s10584-011-0148-z.
- 836 Wang XL and VR Swail. 2001. Changes of extreme wave heights in Northern Hemisphere oceans  
837 and related atmospheric circulation regimes. *J. Clim.* **14**:2204 - 2220.

838 Wyrтки K. 1965. The annual and semiannual variation of Sea Surface Temperature in the North  
839 Pacific Ocean. *Limnology and Oceanography* **10** :307–313.

840 Young EF and JT Holt. 2007. Prediction and analysis of long-term variability of temperature and  
841 salinity in the Irish Sea. *Journal of Geophysical Research* **112** (C1). doi:C01008.  
842 10.1029/2005JC003386.

843 Zhang X, LA Vincent, WD Hogg and A Niitsoo. 2000. Temperature and precipitation trends in  
844 Canada during the 20th century. *Atmos. Ocean* **38**:395-429.

845 Zhang X et al. 2005. Trends in Middle East climate extreme indices from 1950 to 2003. *J.*  
846 *Geophys. Res.* **110**, D22104, doi:10.1029/2005JD006181.

climate model	Institute	ocean model	ocean model resolution	atmospheric model	atmospheric model resolution	grid topography around Brittany
IPSL-LR	IPSL, France	NEMO-ORCA2	2°x2°	LMDz	1.875°x3.75°	No English Channel, England and Ireland are connected to the continent.
IPSL-MR	IPSL, France	NEMO-ORCA2	2°x2°	LMDz	1.25°x2.5°	No English Channel, England and Ireland are connected to the continent.
CNRM-CM5	CNRM, France	NEMO-ORCA1	1°x1°	Arpege-Climate	1.4°x1.4°	realistic
ICHEC EC-EARTH	European consortium (29 institutes)	NEMO-ORCA1	1°x1°	IFS	1.125°x1.125°	realistic
Had-CM3	Met Office Hadley center, England	HadOM3	1.25°x1.25°	HadAM3	2.45°x3.75°	No English Channel, England and Ireland are connected to the continent. No breton tip.
HadGEM2-CC	Met Office Hadley center, England	HadGOM2	0.3°-1°x1°	HadGAM2	1.25°x1.875°	No English Channel, England and Ireland are connected to the continent. No breton tip.
HadGEM2-ES	Met Office Hadley center, England	HadGOM2	0.3°-1°x1°	HadGAM2	1.25°x1.875°	No English Channel, England and Ireland are connected to the continent. No breton tip.
MPI-LR	MPI, Germany	MPI-OM	1°x1.4°	ECHAM6	1.875°x1.875°	realistic
MPI-P	MPI, Germany	MPI-OM	1°x1.4°	ECHAM6	1.875°x1.875°	realistic
MPI-MR	MPI, Germany	MPI-OM	0.5°x0.5°	ECHAM6	1.875°x1.875°	realistic
GFDL-CM3	NOAA, US	MOM4-Tripolar	1°x1°	AM2	2°x2.5°	No English Channel. England connected to the continent.
GFDL-ESM2G	NOAA, US	TOPAZ-Tripolar	1°x1°	AM2	2°x2.5°	realistic
GFDL-ESM2M	NOAA, US	MOM4-Tripolar	1°x1°	AM2	2°x2.5°	No English Channel. England connected to the continent.

Tab1 : CMIP5 climate models used in the study. Name of the global model, names and resolutions of the ocean and atmosphere models, characteristics of the ocean model horizontal grid around Brittany.

Characteristic	Indice	Definition	Computing methodology (for each year)
Mean seasonal cycle	I1	annual mean	average of the 365-day time series
	I10	winter mean (DJF)	average of the 90-day time series (December-January-February)
	I11	spring mean (MAM)	average of the 90-day time series (March-April-May)
	I12	summer mean (JJA)	average of the 90-day time series (June-July-August)
	I13	autumn mean (SON)	average of the 90-day time series (September-October-November)
Seasonal extremes and amplitude	I2	annual minimum	preprocessing of the 365-day time series (see note in table caption); computation of the annual minimum.
	I3	annual maximum	preprocessing of the 365-day time series (see note in table caption); computation of the annual maximum.
	I4	annual amplitude	difference between the annual maximum and the annual minimum.
Seasonal time course	I5	date of the minimum annual temperature	preprocessing of the 365-day time series (see note in table caption); day of the year for which the temperature is minimum.
	I6	date of the maximum annual temperature	preprocessing of the 365-day time series (see note in table caption); day of the year for which the temperature is maximum.
	I7	date of the spring onset	preprocessing of the 365-day time series (see note in table caption); day at which the current increasing temperature is equal to its annual mean (0-phase time)
	I8	date of the autumn onset	preprocessing of the 365-day time series (see note in table caption); day at which the current decreasing temperature is equal to its annual mean (pi-phase time)
	I9	duration of the warm season	preprocessing of the 365-day time series (see note in table caption); length of the within-year period when the temperature is higher than its annual mean.

**Tab. 2** Presentation of indices. Characteristics, number, definition, computing methodology applied for each year. A preprocessing<sup>1</sup> has to be applied for each year to the 365-day times series before the calculation of indices I2 to I9, following Wyrtki (1965) and Saulquin and Gohin (2010).

<sup>1</sup>For each year, the 365-day time series is fitted with a least-square algorithm to a biharmonic signal of the form

$$T = T_0 + T_1 \cos(\omega t - \phi_1) + T_2 \cos(2 \times \omega t - \phi_2)$$

where T is the temperature,  $\omega = \frac{2\pi}{\tau}$  the omega-frequency with  $\tau=365$  days, and t the time (in days) starting

from the beginning of January.  $T_0$  is the average annual temperature,  $T_1$  and  $T_2$  are the amplitudes and  $\phi_1$  and  $\phi_2$  the phases of the annual and semi-annual harmonics, respectively. For each year, the coefficients  $T_0$ ,  $T_1$ ,  $T_2$ ,  $\phi_1$  and  $\phi_2$  that best fit the 365-day time series are estimated and a biharmonic SST signal reconstructed, with a daily time resolution. The biharmonic SST signal is used to compute the yearly value of the indices I2 to I9. The indices I7 to I9 are estimated using the 0-phase and pi-phase time variables defined in Eliseev and Mokhov (2003), derived from the annual cycle amplitude-phase characteristic method.

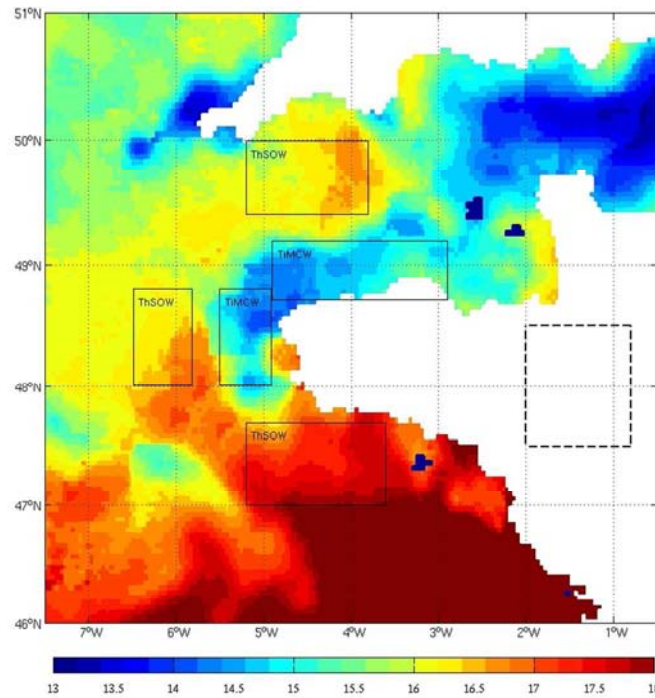


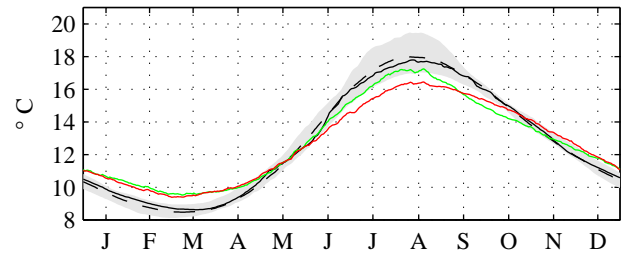
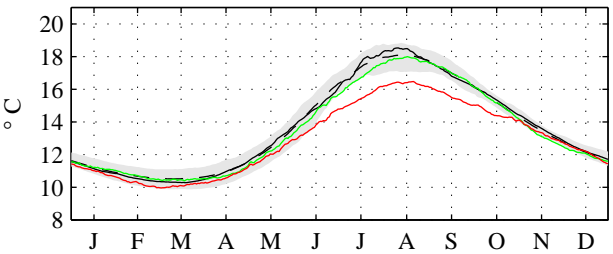
Figure 1: Snapshot of the SST on 18th June 2003 from Ifremer satellite-derived data. Selected ThSOW and TiMCW areas in the Iroise Sea, the English Channel and the Bay of Biscay (solid line). A typical grid cell size for CMIP5 models (dashed line), representative of the grid cell size of 10 models over the 13 models of the study.

423x317mm (72 x 72 DPI)

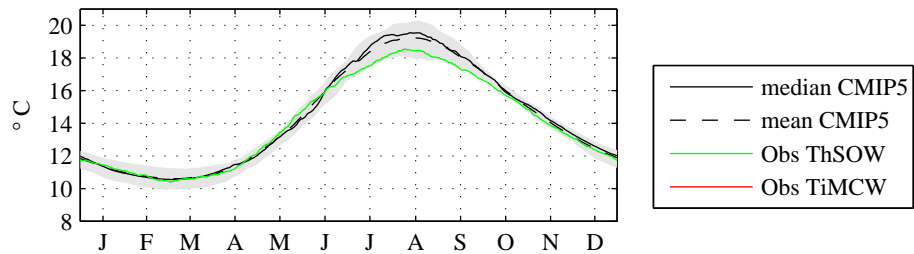
Peer

Iroise Sea

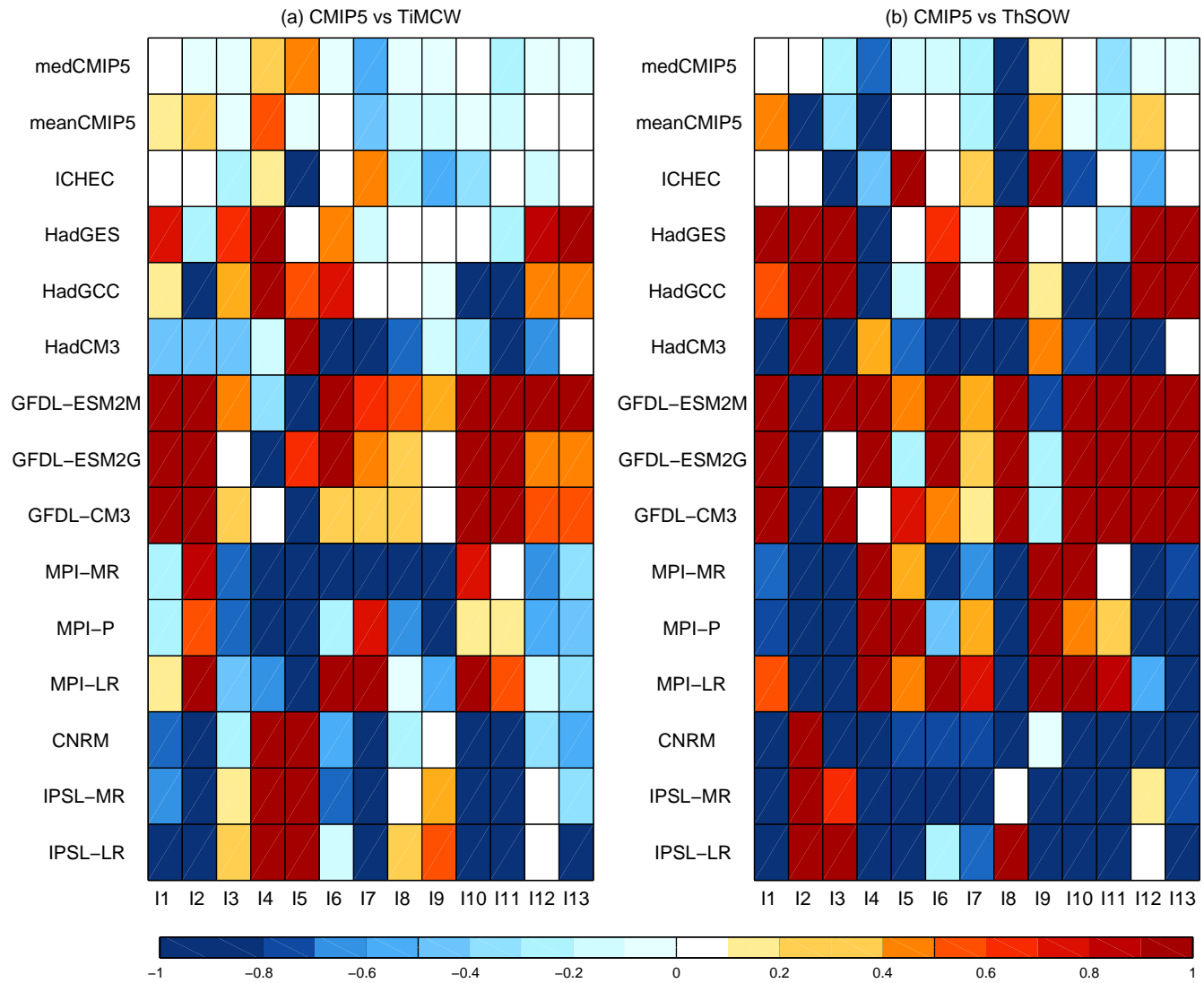
English Channel



Bay of Biscay



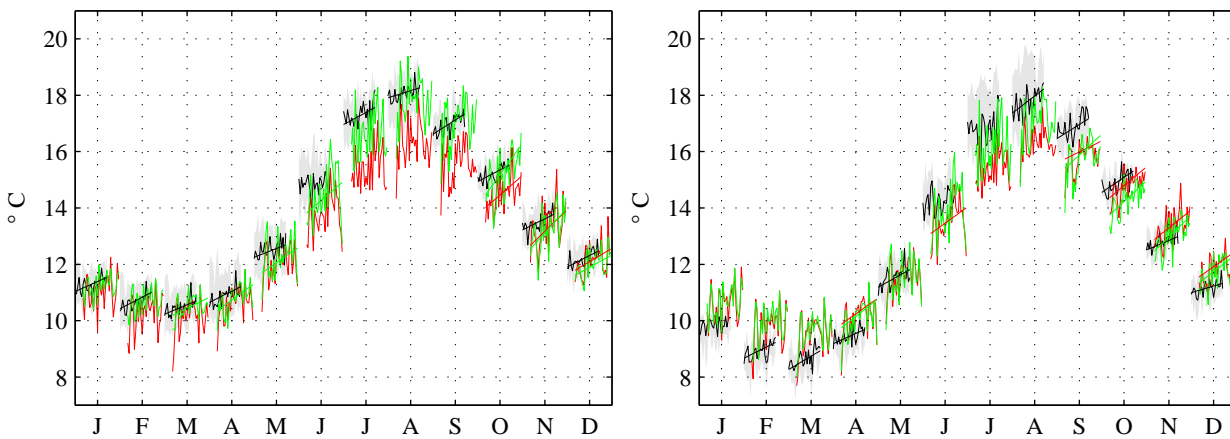
13



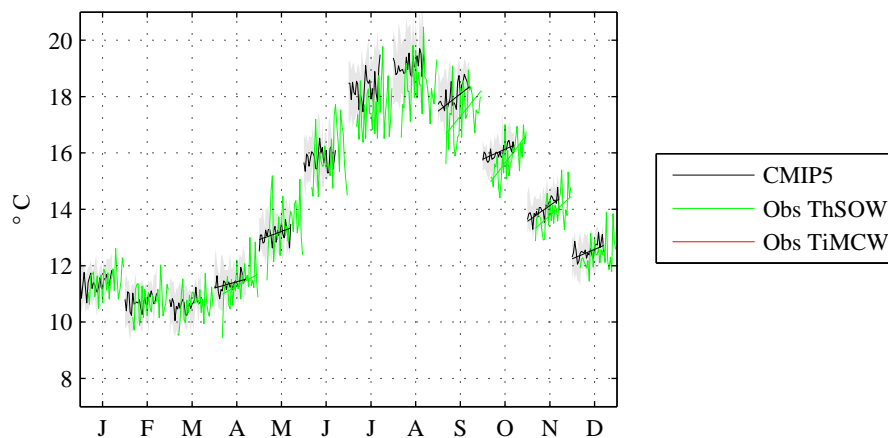
Peer

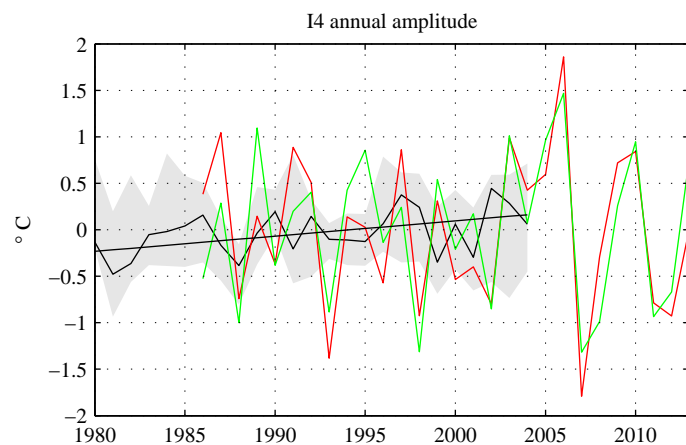
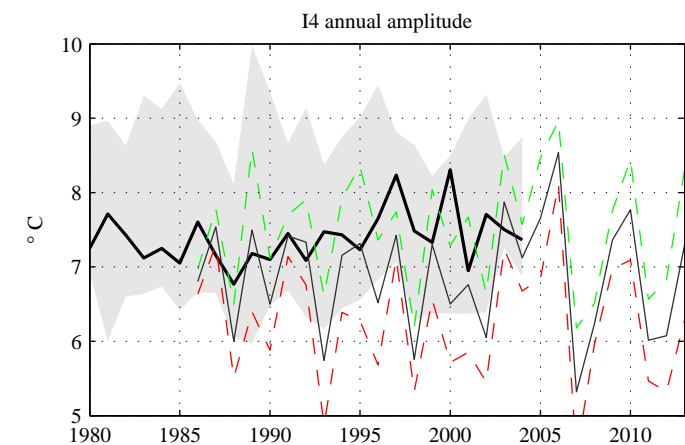
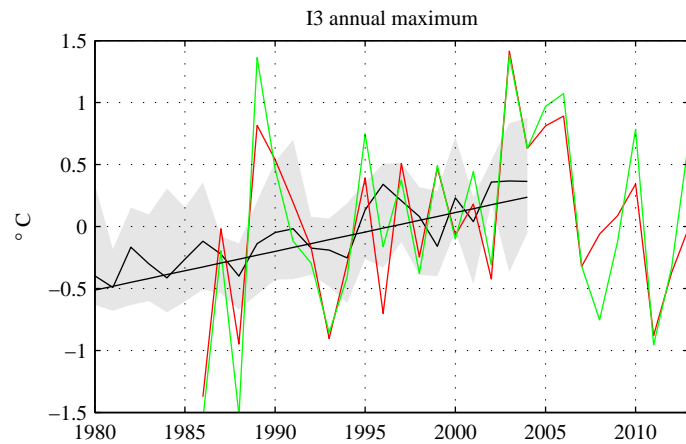
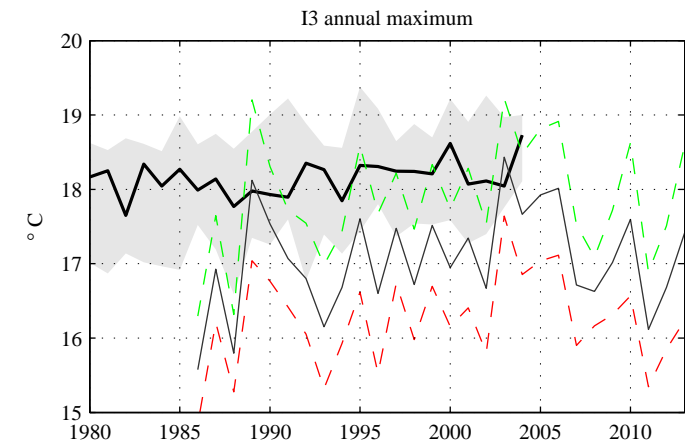
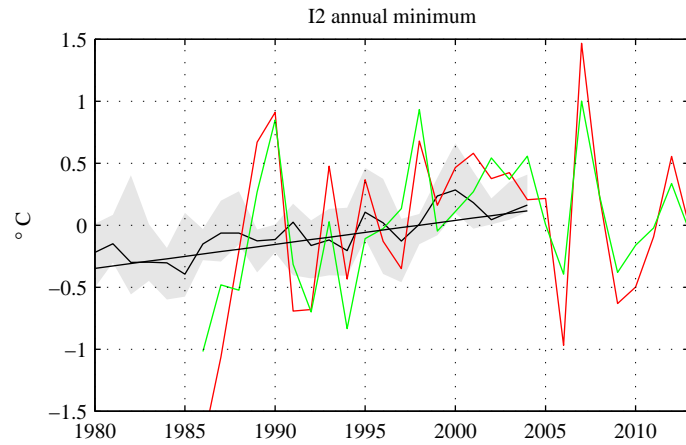
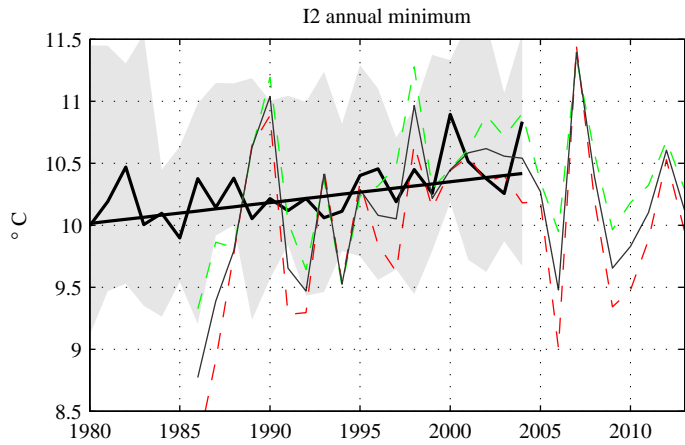
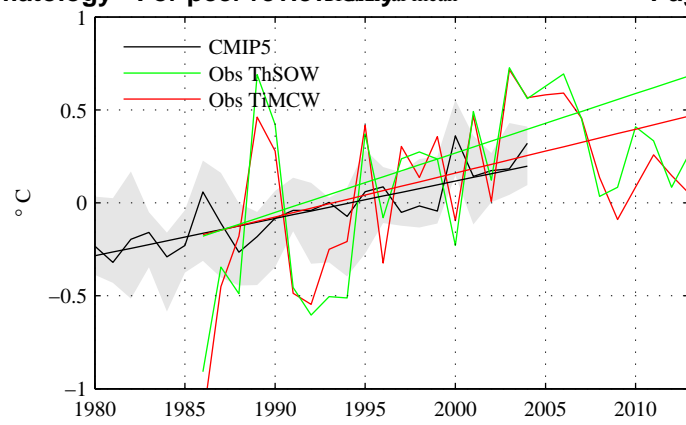
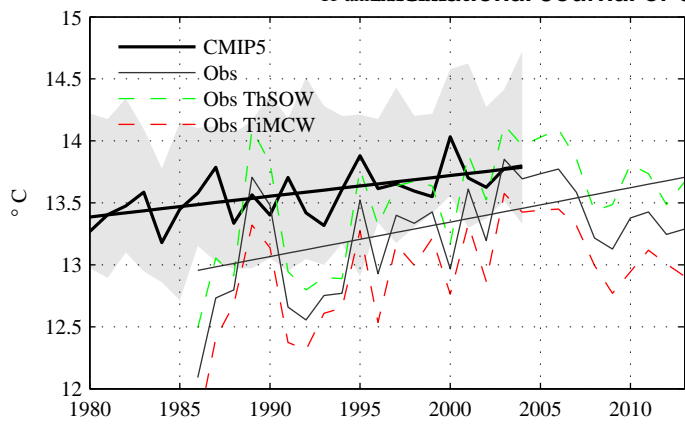
Iroise Sea

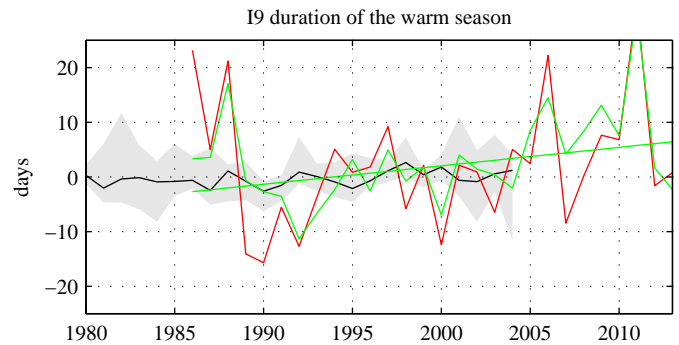
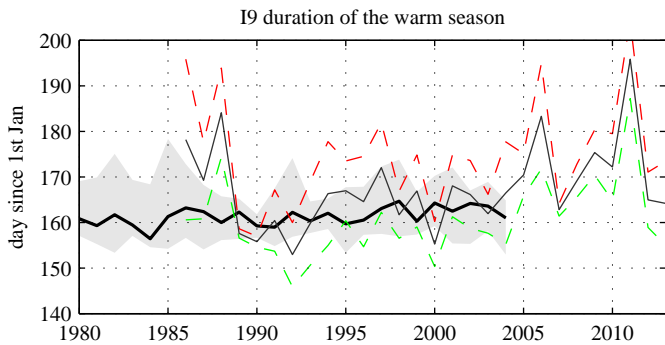
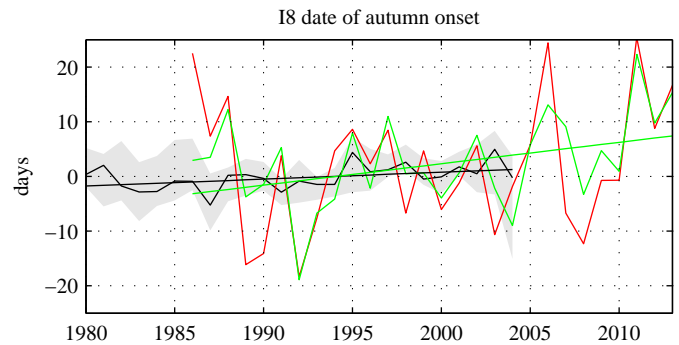
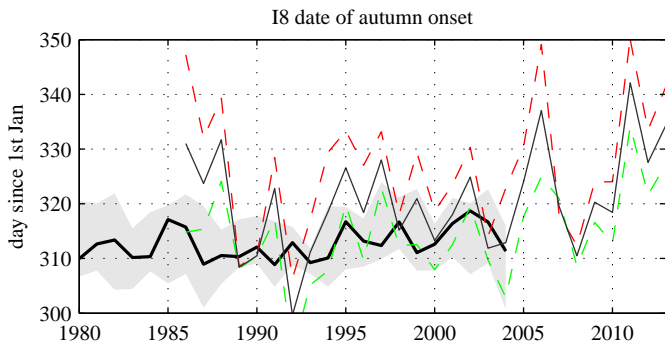
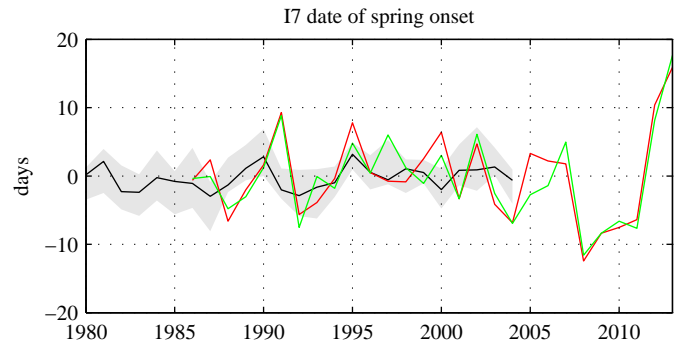
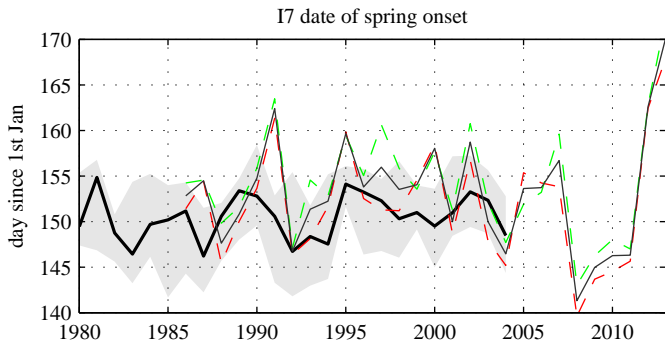
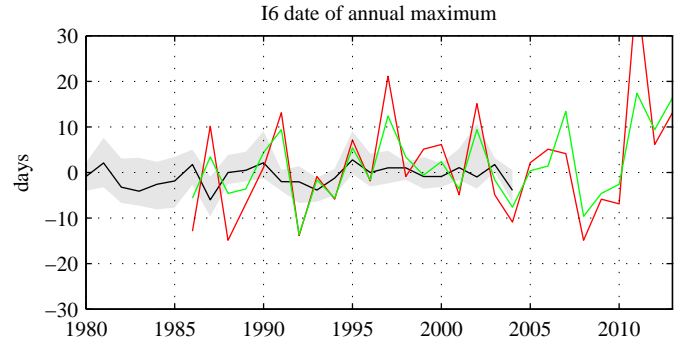
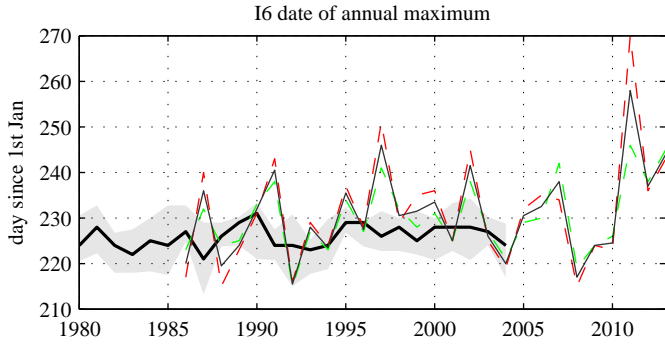
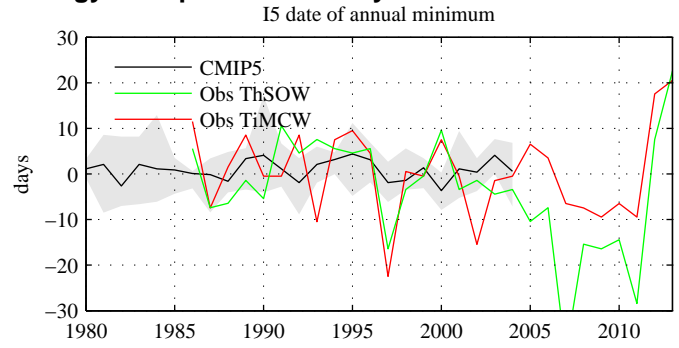
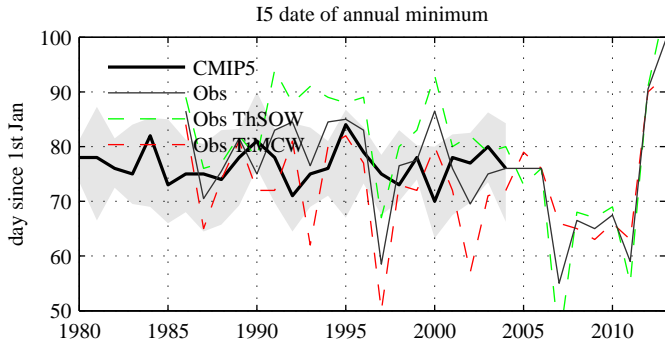
English Channel

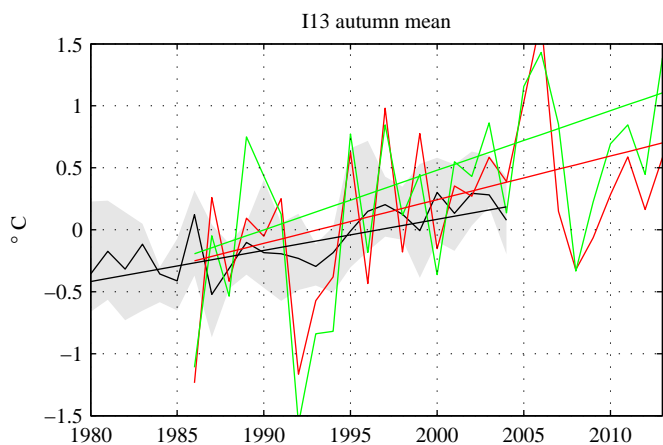
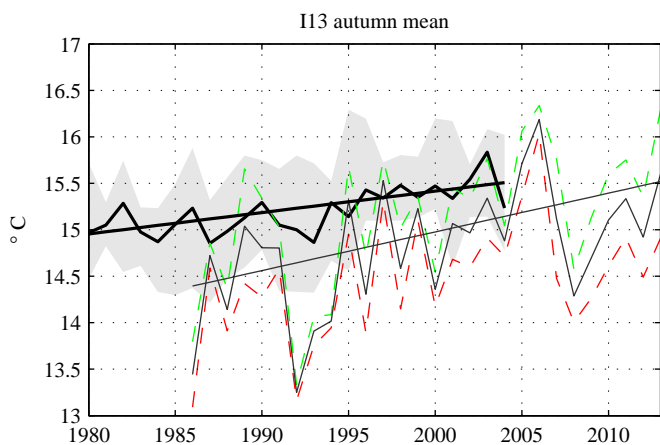
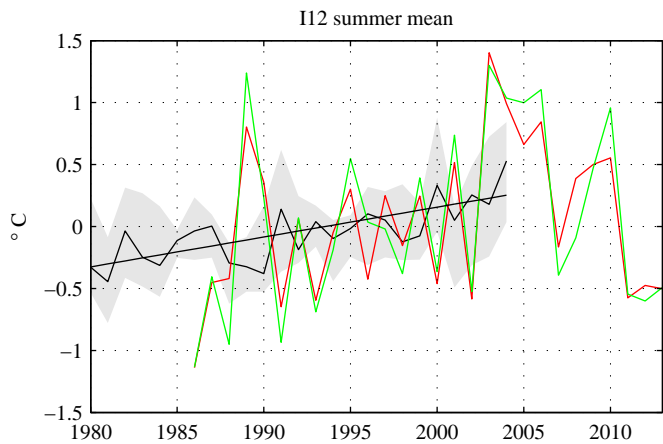
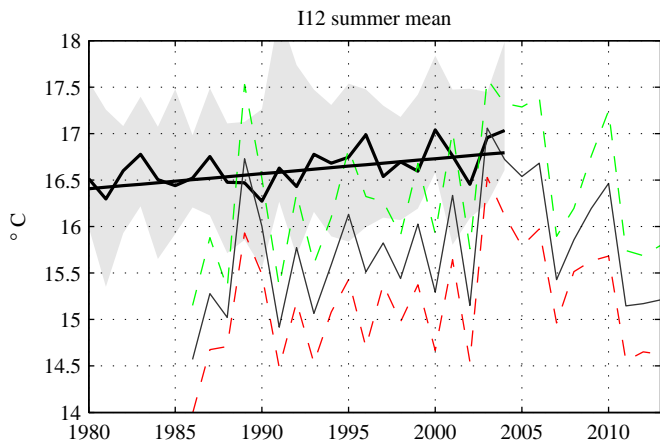
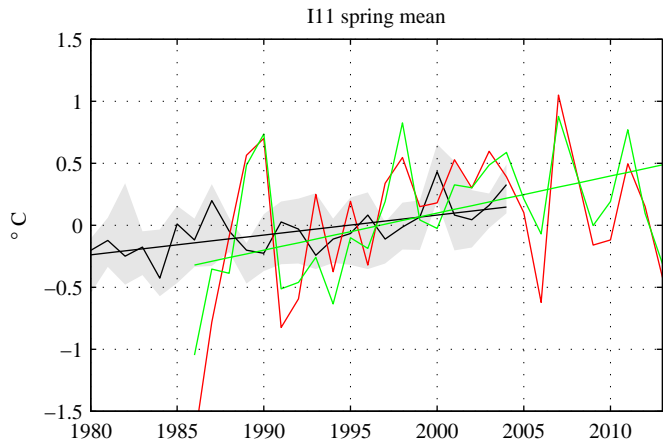
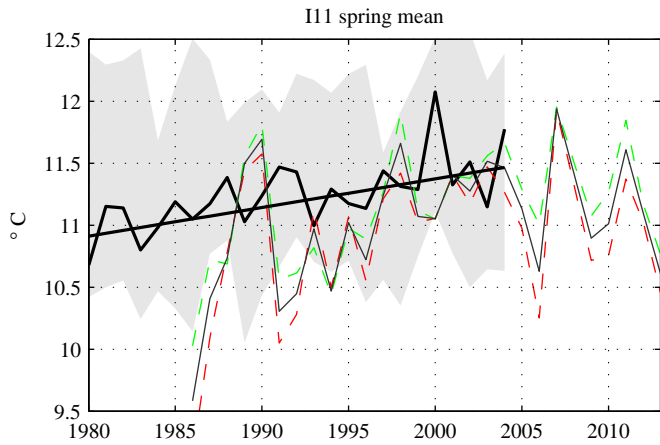
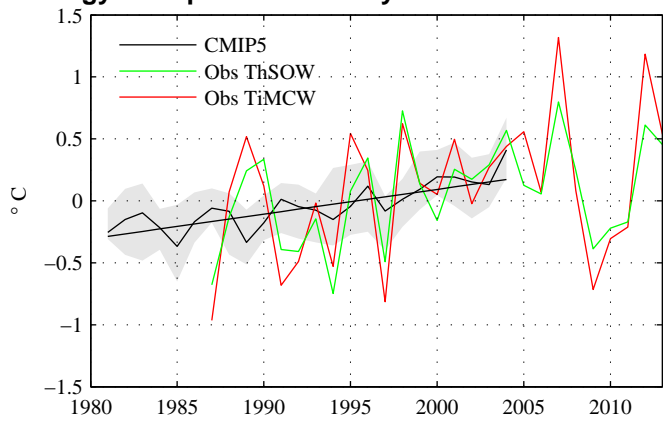
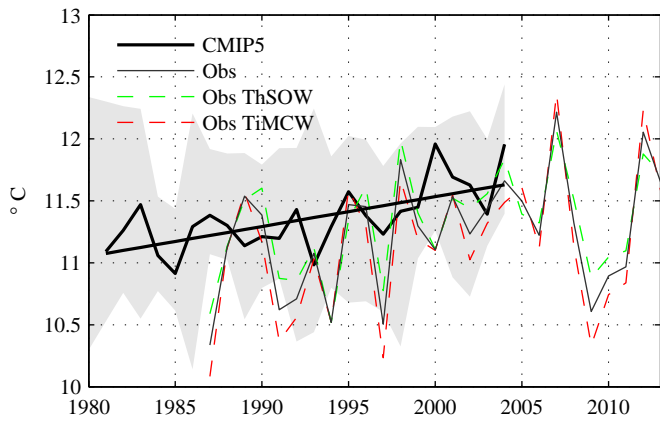


Bay of Biscay

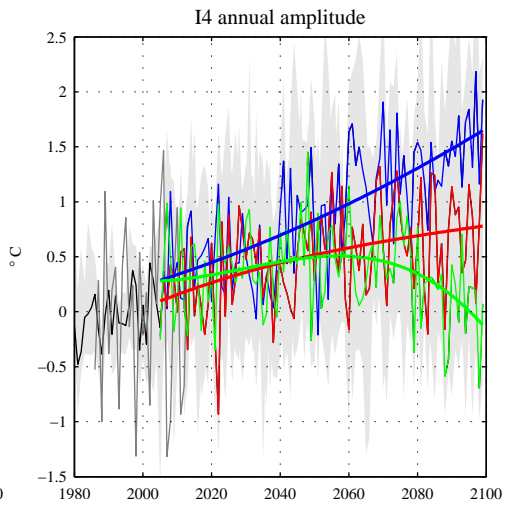
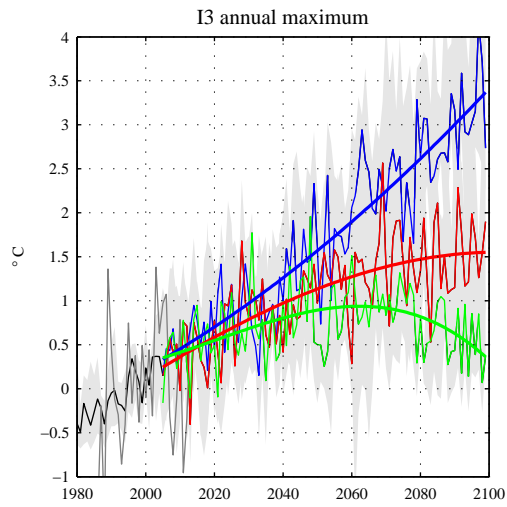
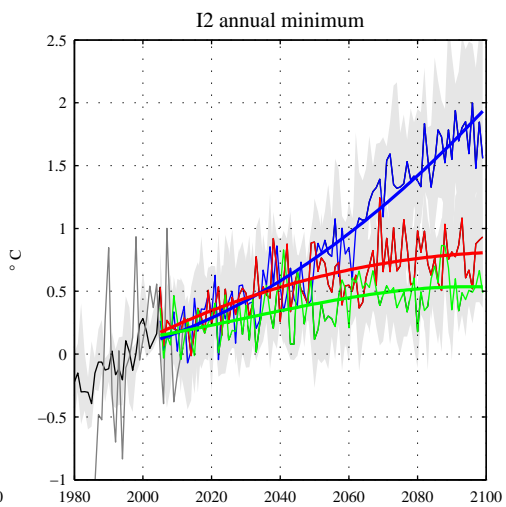
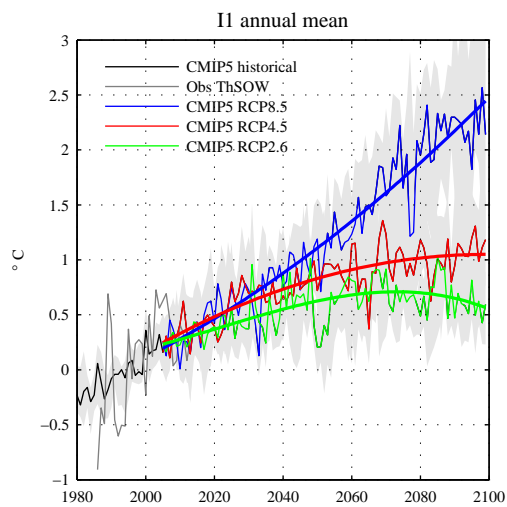








Peer



Peer

